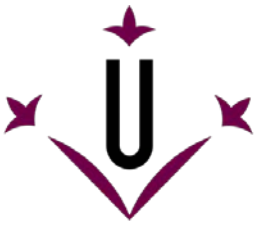

A genome-wide transcriptional study reveals that iron deficiency inhibits the yeast TORC1 pathway

Antonia María Romero[1,*], Lucía Ramos-Alonso[1], Sandra Montellá-Manuel[2], José García-Martínez[3,5], María Ángeles de la Torre-Ruiz[2], José Enrique Pérez-Ortín[4,5,**], María Teresa Martínez-Pastor[4,#] and Sergi Puig[1,#]

[1] Departamento de Biotecnología, Instituto de Agroquímica y Tecnología de Alimentos (IATA), Consejo Superior de Investigaciones Científicas (CSIC), E-46980, Paterna, Valencia, Spain.

[2] Department of Basic Medical Sciences, IRB-Lleida, University of Lleida, E-25198, Lleida, Spain.

[3] Departamento de Genética, Universitat de València, E-46100, Burjassot, Valencia, Spain.

[4]Departamento de Bioquímica y Biología Molecular, Universitat de València, E-46100, Burjassot, Valencia, Spain.

[5]ERI Biotecmed, Universitat de València, E-46100, Burjassot, Valencia, Spain.

Present addresses:

*Department of Chemistry and Molecular Biology, University of Gothenburg, Gothenburg, Sweden.

** SciLifeLab, Department of Microbiology, Tumor, and Cell Biology, Karolinska Institute, Tomtebodavägen 23, SE-171 21, Stockholm. Sweden

Corresponding authors. Tel: (+34) 963 900 022; Fax: (+34) 963 636 301; Email: spuig@iata.csic.es and maria.teresa.martinez@uv.es

Keywords: iron deficiency / transcription / TOR / yeast /RNA polymerases

Abstract

Iron is an essential micronutrient that participates as a cofactor in a broad range of metabolic processes including mitochondrial respiration, DNA replication, protein translation and lipid biosynthesis. Adaptation to iron deficiency requires the global reorganization of cellular metabolism directed to optimize iron utilization. The budding yeast *Saccharomyces cerevisiae* has been widely used to characterize the responses of eukaryotic microorganisms to iron depletion. In this report, we used a genomic approach to investigate the contribution of transcription rates to the modulation of mRNA levels during adaptation of yeast cells to iron starvation. We reveal that a decrease in the activity of all RNA polymerases contributes to the down-regulation of many mRNAs, tRNAs and rRNAs. Opposite to the general expression pattern, many genes including components of the iron deficiency response, the mitochondrial retrograde pathway and the general stress response display a remarkable increase in both transcription rates and mRNA levels upon iron limitation, whereas genes encoding ribosomal proteins or implicated in ribosome biogenesis exhibit a pronounced fall. This expression profile is consistent with an irreversible activation of the environmental stress response. The phosphorylation of multiple regulatory factors strongly suggests that the conserved nutrient signaling pathway TORC1 is inhibited during the progress of iron deficiency. These results suggest an intricate crosstalk between iron metabolism and the TORC1 pathway that should be considered in many disorders.

Highlights

1) The activity of yeast RNA polymerases decreases in response to iron deficiency.
2) Iron depletion activates the yeast environmental stress response.
3) The TORC1 pathway is inhibited during the progress of iron deficiency
4) Iron starvation transcriptionally activates the mitochondrial retrograde pathway.

1. Introduction

Iron is a vital micronutrient for all forms of eukaryotic life because it participates as a redox cofactor in fundamental cellular processes. Although iron is abundant, its bioavailability is highly restricted under aerobic conditions because of the insolubility of ferric iron at physiological pH. Thus, the acquisition and maintenance of sufficient iron levels is a challenge for living organisms, which have evolved sophisticated mechanisms to modulate iron homeostasis. Indeed, iron deficiency anemia is the most widespread nutritional disorder in humans, estimated to affect more than two billion people with a high prevalence in children and women of childbearing age [1]. Moreover, iron acquisition and regulation within the extremely poor-iron environment of the host is crucial for the progress of microbial infections [2-4]. The budding yeast *Saccharomyces cerevisiae* has proved to be a reliable model to identify and characterize mechanisms of adaptation to iron deficiency. In response to iron scarcity, the Aft1 and Aft2 transcription factors accumulate into the nucleus of yeast cells, bind to iron responsive elements (FeREs), and activate the expression of ~35 genes known as the iron regulon, which are mainly involved in the acquisition of extracellular iron and the mobilization and recycling of intracellular iron. Aft1 and Aft2 also activate the transcription of the mRNA-binding protein Cth2 (also known as Tis11), which promotes the post-transcriptional degradation of multiple mRNAs within the electron transport chain and the tricarboxylic acid cycle, in order to limit iron consumption in mitochondrial respiration (reviewed in [5-8]).

The conserved target of rapamycin (TOR) serine/threonine kinase and its namesake pathway, which were first discovered in yeast, control cell growth and

metabolism in response to environmental cues such as nutrient levels, cell integrity, stress or energy status (reviewed in [9-11]). The TOR kinase can function in two different complexes, TORC1 and TORC2, which are conserved from yeast to mammals. The yeast TORC1 complex is composed of Tor1 or Tor2 kinase, and the Lst8, Kog1 and Tco89 proteins. The two major downstream effectors of the TORC1 complex are the Sch9 kinase and the phosphatase complex Tap42-PP2A. When the environmental conditions are favorable, the TORC1 pathway promotes ribosome biogenesis and protein translation by favoring the expression of ribosomal proteins (RPs), ribosome biogenesis (RiBi) factors, rRNAs and tRNAs at multiple levels [9]. Under these conditions, TORC1 enhances rRNA expression by inhibiting the proteasome-dependent degradation of Rrn3, the activating factor of the RNA polymerase I (RNA Pol I) [12], and tRNA transcription by regulating the phosphorylation stage of the RNA polymerase III (RNA Pol III) repressor Maf1. However, upon nutrient limitation, or in the presence of the lipophilic drug rapamycin, the inactivation of TORC1 provokes a decrease in the phosphorylation of Sch9, and subsequently of Stb3 and Dot6/Tod6 transcription factors, which, together with the Rpd3L histone deacetylase complex, repress the transcription of RP and RiBi genes [9, 13]. Under these conditions, Sfp1, an activator of RP and RiBi genes and a direct target of TORC1, is inactivated by dephosphorylation and exported to the cytoplasm (reviewed in [9]).

The mitochondrial retrograde (RTG) response facilitates the production of multiple biosynthetic intermediates. This signaling pathway communicates mitochondria with the nucleus, activating the expression of several nuclear genes that are necessary for the synthesis of glutamate and other anabolic precursors of amino acids through anaplerotic reactions. These genes include *CIT2*, the

peroxisomal isoform of citrate synthase that produces citrate as part of the glyoxylate cycle, and the genes encoding the enzymes of the three first steps in the tricarboxylic acid (TCA) cycle: *CIT1*, coding for the mitochondrial isoform of citrate synthase; *ACO1*, aconitase, and *IDH1/2*, encoding NAD^+-dependent isocitrate dehydrogenase (reviewed in [14]), which enable cells to maintain glutamate and glutamine supplies when mitochondria are dysfunctional and cells are respiratory deficient through the synthesis of α-ketoglutarate. The retrograde signaling requires the nuclear translocation of a heterodimeric transcription factor constituted by Rtg1 and Rtg3 proteins, which occurs after the Rtg2-dependent partial dephosphorylation of Rtg3. The TORC1 complex negatively regulates retrograde signaling through its component Lst8, acting both upstream and downstream of Rtg2 (reviewed in [14, 15]).

Previous genome-wide studies have analyzed the changes in mRNA levels that *S. cerevisiae* undergoes in response to iron deficiency [16-18]. The information obtained from these global studies is nonetheless limited, as it involves the measurement of steady-state mRNA amounts (RA). To assess the contribution of transcription to the adaptation to iron limitation, we have used the genomic run-on (GRO) technique [19] to determine the transcription rate (TR) for the entire yeast transcriptome during the progress from mild to severe iron deficiency. Our data uncover new insights onto the molecular mechanisms involved in the adaptation to iron deprivation, including the activation of the environmental stress response (ESR) and the mitochondrial retrograde response, and a decrease in the transcription rates of RP and RiBi genes, which support the inhibition of the TORC1 pathway.

2. Materials and methods

2.1. Yeast strains, plasmids and growth conditions. The yeast strains used in this study are listed in Table S1. The pCM64-P_{ACO1}-lacZ reporter plasmid was made by the insertion of a 613-bp PCR amplified fragment from the *ACO1* promoter region into the BglII-BamHI sites of pCM64 vector (from Charles Moehle). The Sfp1-GFP plasmid was constructed by amplifying *SFP1* sequence flanked by SalI and SmaI restriction sites, digestion and cloned into pUG35 plasmid. Yeast W303 cells were cultivated in 600 mL of SC medium for at least 15 hours to reach early exponential phase (OD_{600} = 0.2). Then, 100 μM of the Fe^{2+}-specific chelator bathophenanthroline disulfonic acid (BPS; Sigma) was added, and different aliquots were isolated at 0, 10, 30, 90, 180 and 360 minutes after iron limitation. In the case of yeast cells from the BY4741 or other backgrounds, 3 mL overnight precultures were used to inoculate 50 mL of SC (+Fe) or SC + 100 μM BPS cultures (-Fe), and 10 mL aliquots were taken at the specified times. For microscopy, cultures were grown at 30ºC in SC to OD_{600} = 0.6. Then, yeast cells were washed four times in either SD or SD + 100 μM BPS. Half of the cells were transferred to fresh SD medium or alternatively to SD + 100 μM BPS (-Fe) at OD_{600} = 0.2. Cultures were grown for 8 hours in continuous shaking. Samples were taken for observation in an Olympus Bx51 fluorescence microscope.

2.2. Determination and analyses of transcription rates and mRNA levels. To determine the TR and RA of each gene on a genome-wide scale, we followed the GRO and mRNA measurement protocols previously described [19], except that cells were frozen after collection and the reverse transcription of mRNA was

carried out using an oligo-d$(T)_{15}$VN (V means A, G, or C; N means A, G, C, or T) instead of random primers. Three biologically independent replicates were performed for each experiment. Quantification and normalization of the data were performed as reported [19]. Changes in the normalized median values of TR and RA were evaluated by cluster analysis with WebMeV (Multiple Experiment Viewer) web server (http:/mev.tm4.org). To determine cluster composition, we used a k-means clustering with k=10 and Euclidean distance. After obtaining the heatmap, the color code was used to visually select the gene clusters. Finally, we used the Gene Ontology enRIchment anaLysis and visuaLizAtion tool (http://cbl-gorilla.cs.technion.ac.il) to ascertain the statistical significance of the enrichment of clusters in specific gene ontology (GO) categories. We determined adjusted *p-values* with FDR multiple correction.

2.3. Total poly(A) RNA measurements. We used a dot-blot procedure to determine the poly(A) mRNA/cell as previously described [19].

2.4. RNA analyses. Total yeast RNA isolation, reverse transcription and quantitative PCR (RT-qPCR) were performed as previously described [20]. Specific primer pairs were used for the qPCR (listed in Table S2). The data and error bars represent the relative average and standard deviations of three independent biological samples.

2.5. Protein analyses. Yeast proteins were extracted and analyzed by Western blot as previously reported [20], except in the case of Sch9 and Maf1 protein phosphorylations, which were studied with specific procedures [21-23]. Since Sch9 protein is around 100 KDa, a chemical fragmentation of Sch9-HA protein was performed with NTCB (2-nitro-5-thiocyanatobenzoic acid), which cyanylates

cysteine residues that under alkaline conditions are followed by chain cleavage at the modified residues. Chromatin immunoprecipitation (ChIP) assays were performed to determine RNA Pol II binding to Rtg1-regulated gene promoters as described [24]. Cell extracts for ChIP were incubated with Dynabeads Pan Mouse IgG (Invitrogen), previously bound to a monoclonal mouse anti-Rpb1 antibody (clone 8WG16, Covance), and DNA was purified with the High Pure PCR Product Purification Kit (Roche). The primers used for the RT-qPCR analyses are listed in Appendix Table S2. The primary antibodies used in this study included anti-Rpb1 (1:20,000 dilution; clone 8WG16, Covance), anti-Rpb1-Ser2-Phosphorylated (1:20,000 dilution; Abcam), anti-HA (1:5,000 dilution; 3F10**,** Sigma), anti-Rpa190A (1:20,000 dilution; from Olga Calvo), anti-GFP (1:10,000 dilution; Roche), anti-Rps6 (1:1,000 dilution; Cell Signaling Technology), anti-Rps6-Ser235/Ser236 (1:1,000 dilution; Cell Signaling Technology), anti-Maf1 (1:10,000 dilution; from Olivier Lefebvre) and anti-Pgk1 (1:10,000 dilution; 22C5D8, Invitrogen). Immunoblot images were obtained with an ImageQuant LAS 4000 mini Biomolecular Imager (GE Healthcare Life Sciences), and protein levels were quantified with ImageQuant TL analysis software (GE Healthcare Life Sciences).

2.6. Determination of glucose and ethanol concentrations. Glucose and ethanol concentrations in all the supernatant samples were determined by HPLC in a Surveyor Plus Chromatograph (Thermo Fisher Scientific, Waltham, MA) equipped with a refraction index detector, an autosampler and a UV-Visible detector. Each sample was analyzed in duplicate.

2.7. Miscellaneous. Cell median volumes were determined with a Coulter Counter Z (Beckman Coulter, USA). Rrp12-GFP, Sfp-GFP and Rtg1-GFP expressing cells were stained with 4’,6-diamidino-2-phenylindole (DAPI) and visualized in an

Axioskop 2 fluorescence microscope (Zeiss), and images were captured with a SPOT camera (Diagnostic Instruments). β-Galactosidase activity was measured as previously described [24]. Total intracellular iron levels were determined as previously described [25]. Tailed t-student tests were applied to evaluate statistical significance.

2.8. Statistical analyses. To evaluate statistical significance, tailed t-student tests were applied. The asterisk (*) indicates statistically significant differences with p-value < 0.05.

2.9. Accession numbers. The Gene Expression Omnibus (GEO) accession number for the whole experiment is GSE127875.

3. Results

3.1. General responses during the adaptation to iron deficiency

Various studies have shown that the yeast *S. cerevisiae* alters the steady-state levels of many transcripts in response to nutritional or genetic iron deficiencies [16-18]. However, little is known about the relative contribution of transcription to the abundance of specific mRNAs upon iron scarcity. To address this question, we determined the TR and the RA per cell of the entire yeast genome during the progress of iron deficiency. We cultivated a haploid prototroph W303 yeast strain to early exponential phase (A_{600} = 0.3; $7 \cdot 10^6$ cells/mL), and then we added 100 μM of bathophenanthroline disulfonate (BPS), a widely used Fe^{2+}-specific chelator that limits extracellular iron bioavailability. With the aim of deciphering both early and late responses to iron deprivation, aliquots were collected up to six hours after iron limitation. Growth rate slightly decreased after 6 hours of iron depletion, but cells continued duplicating up to 24 hours under these conditions (Figure S1A and S1B). Metabolite analyses showed a mild decrease in glucose concentration and increase in ethanol levels (Figure S1C). No important changes were observed in cellular volume during the progress of the experiment (Figure S1D). Intracellular iron levels displayed a 14% decrease in the initial 30 minutes, and further diminished along the progress of the iron depletion (Figure S1E). To quantify the RNA polymerase II (RNA Pol II) TR of each yeast gene, we used the GRO method [19] (Materials and Methods). The whole RNA Pol II TR was obtained from the median of the TR corresponding to all the yeast protein-coding genes, whereas the total RA was determined by hybridization with labeled oligo(dT) [19] (Materials and Methods). The profile of total RA and TR

distinguished three different stages along the iron deficiency (Figure 1A). First, cells experienced an early response to low iron (from 0 to 30 min), in which both total RA and TR decreased. Following this initial stage, the TR and RA increased to peak between 90 and 180 min. Finally, both TR and RA fell and achieved their minimal value after 6 hours of iron depletion (Figure 1A). To obtain some insight into the molecular reasons for these changes in TR, we determined the mRNA and protein levels of the largest subunit of the RNA Pol II complex, Rpb1. Consistently with a decrease in the RNA Pol II TR, both Rpb1 mRNA and protein levels slightly decreased as the iron deficiency advanced (Figure 1B and 1C). Remarkably, the levels of elongating Rpb1, which is transiently phosphorylated at the second serine of the heptapeptide repeat within its carboxy-terminal domain (Rpb1-S_2-P), further diminished (Figure 1C), indicating a stronger defect in elongating RNA Pol II at longer times. Collectively, these results suggest that yeast cells experience important decreases in transcription during the adaptation to iron deficiency.

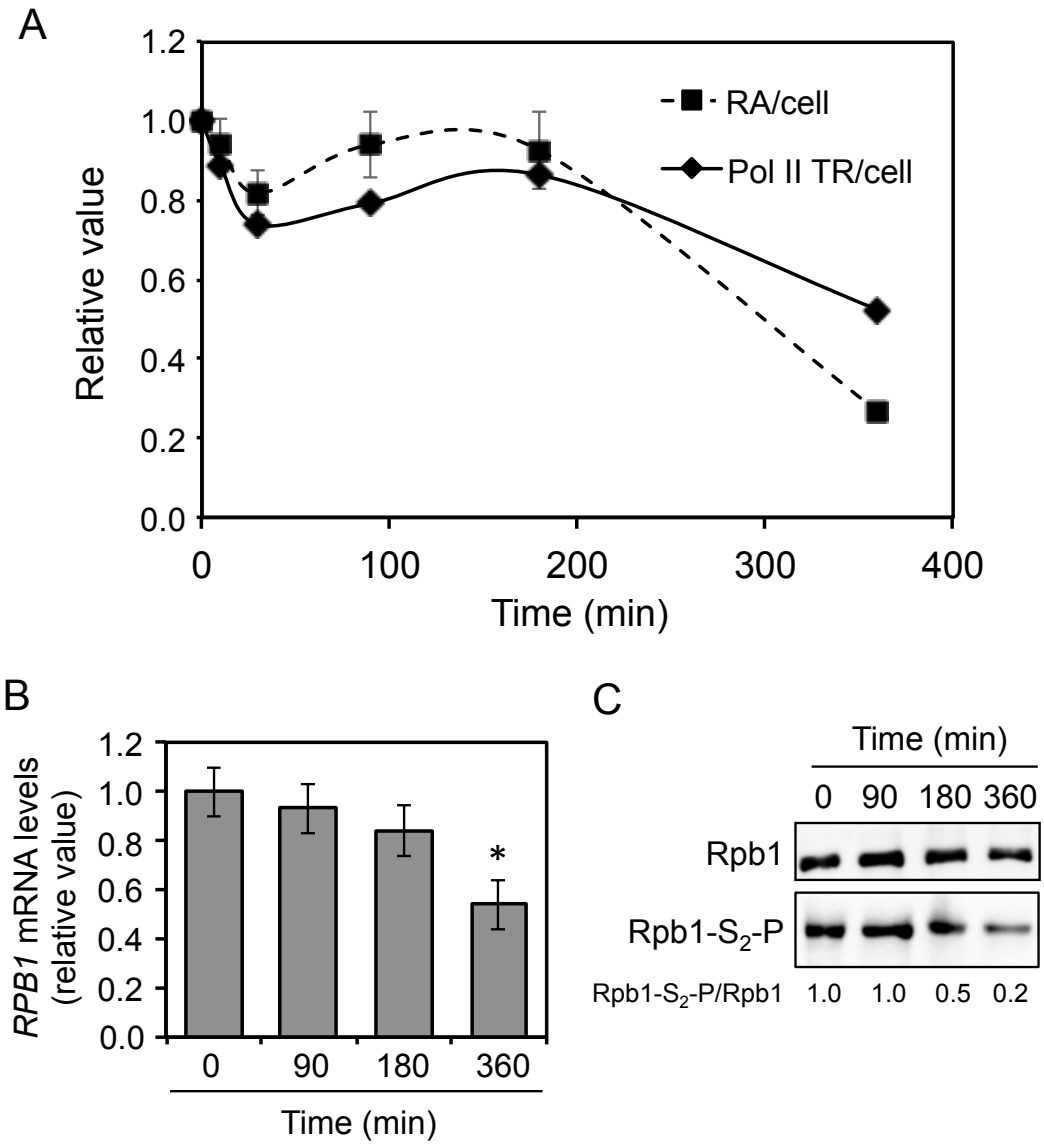

Figure 1. Changes in RNA polymerase II during the progress of iron deficiency. **(A)** RNA Pol II transcription rate (TR) and total poly(A) mRNA (RA) per cell. At time zero, 100 μM BPS was added to W303 cells exponentially growing in SC at 30°C. Aliquots were processed to measure total RA per cell and RNA Pol II TR per cell at the indicated times, (Materials and Methods). The values were referred to their respective values at time zero. The standard deviation of at least three biologically independent replicates is shown. **(B)** *RPB1* mRNA levels were determined by RT-qPCR using specific primers. Average values and standard deviations from at least two independent experiments are shown and referred to those in time zero. **(C)** The levels of total and elongating RNA pol II (Rpb1 and Rpb1-S_2-P, respectively) were determined by Western blot analyses using the anti-Rpb1 antibody that recognizes all the RNA pol II molecules and the anti-Ser2-phosphorylated antibody that measures elongating RNA

pol II. A representative experiment of three independent biological replicates is shown. Protein levels have been quantified and the Rpb1-S_2-P/Rpb1 ratio indicated.

3.2. Identification of gene clusters with coordinated changes in transcription rates and mRNA levels during iron depletion

To identify sets of genes coordinately regulated along the iron deficiency kinetics, we performed gene-clustering analyses according to the experimental TR and RA profiles (Supplementary Data S1). The individual RA values after 6 hours of iron deficiency were not included in these analyses because we obtained no detectable signal. By this method, we classified 4421 genes into 10 different clusters, which were statistically enriched in specific gene ontology (GO) functional categories (Figure 2; Supplementary Data S2; only representative GO categories with $p \leq 10^{-4}$ are indicated). The profile for each cluster was represented (Figure 3). Consistent with the activation of the iron regulon by the Aft1 and Aft2 transcription factors previously reported [16-18], the GO category "iron ion homeostasis" was over-represented in cluster 1 ($p = 3.4 \cdot 10^{-14}$) and cluster 4 ($p = 2.5 \cdot 10^{-5}$), which TR and RA gradually augmented during the time-course of iron deficiency (Figures 2 and 3). For instance, the mRNA levels of *CTH2* mRNA increased 17-fold after 3 hours of iron deprivation (Supplementary Data S2). Cluster 4 also contained the Mga2-dependent transcriptional induction reported for the *OLE1* fatty acid desaturase in response to iron limitation [24]. Interestingly, cluster 2 contained genes whose RA decrease was more pronounced than its drop in TR, suggesting a significant contribution of mRNA decay to its regulation (Figure 3). In fact, the GO category "respiratory electron transport chain" contains multiple targets of the iron-regulated Cth2 mRNA decay factor (Supplementary Data S2). All these results

validated our experimental conditions and, from here onwards, we focused on identifying new functional categories coordinately regulated in response to iron depletion. Cluster 4,, which exhibited an increase in both TR and RA, was enriched in the GO category "cellular response to external stimulus" ($p = 3.9 \cdot 10^{-8}$) (Figures 2 and 3). Cluster 5, over-represented in the GO functional categories "oxidation-reduction process" and "small molecule metabolic process" ($p = 6.6 \cdot 10^{-8}$ and $p = 2.5 \cdot 10^{-5}$, respectively), displayed identical TR and RA patterns with only a slight and transient decrease at 30 min of iron depletion (Figure 3), In addition to cluster 2, clusters 6 to 10 showed an overall decrease in TR (Figure 3). A similar pattern for both TR and RA was observed in cluster 7, with three significative GO categories "organonitrogen compound biosynthetic process", "translation" and "mitochondrial translation" ($p = 7.6 \cdot 10^{-10}$, $p = 1.2 \cdot 10^{-7}$ and $p = 2.8 \cdot 10^{-5}$ respectively). Representative GO categories were also identified in cluster 8 ("nucleic acid metabolic process", $p = 6.8 \cdot 10^{-9}$; and "cell cycle process", $p = 7.9 \cdot 10^{-9}$) and cluster 9 ("endosomal transport", $p = 6.8 \cdot 10^{-9}$; and "protein localization", $p = 8.6 \cdot 10^{-6}$) (Figures 2). Finally, cluster 10 contained two representative GO functional categories: "RNA metabolic process" ($p = 8.6 \cdot 10^{-6}$), and "ribosome biogenesis" ($p = 7.6 \cdot 10^{-39}$). Remarkably, the *p*-value for "ribosome biogenesis" was even lower than the *p*-value obtained for the "iron ion homeostasis" category in cluster 1 (Figure 2). Collectively these results suggest that the modulation of transcription, and to a lower extent mRNA stability, contribute to the response of yeast cells to iron deficiency.

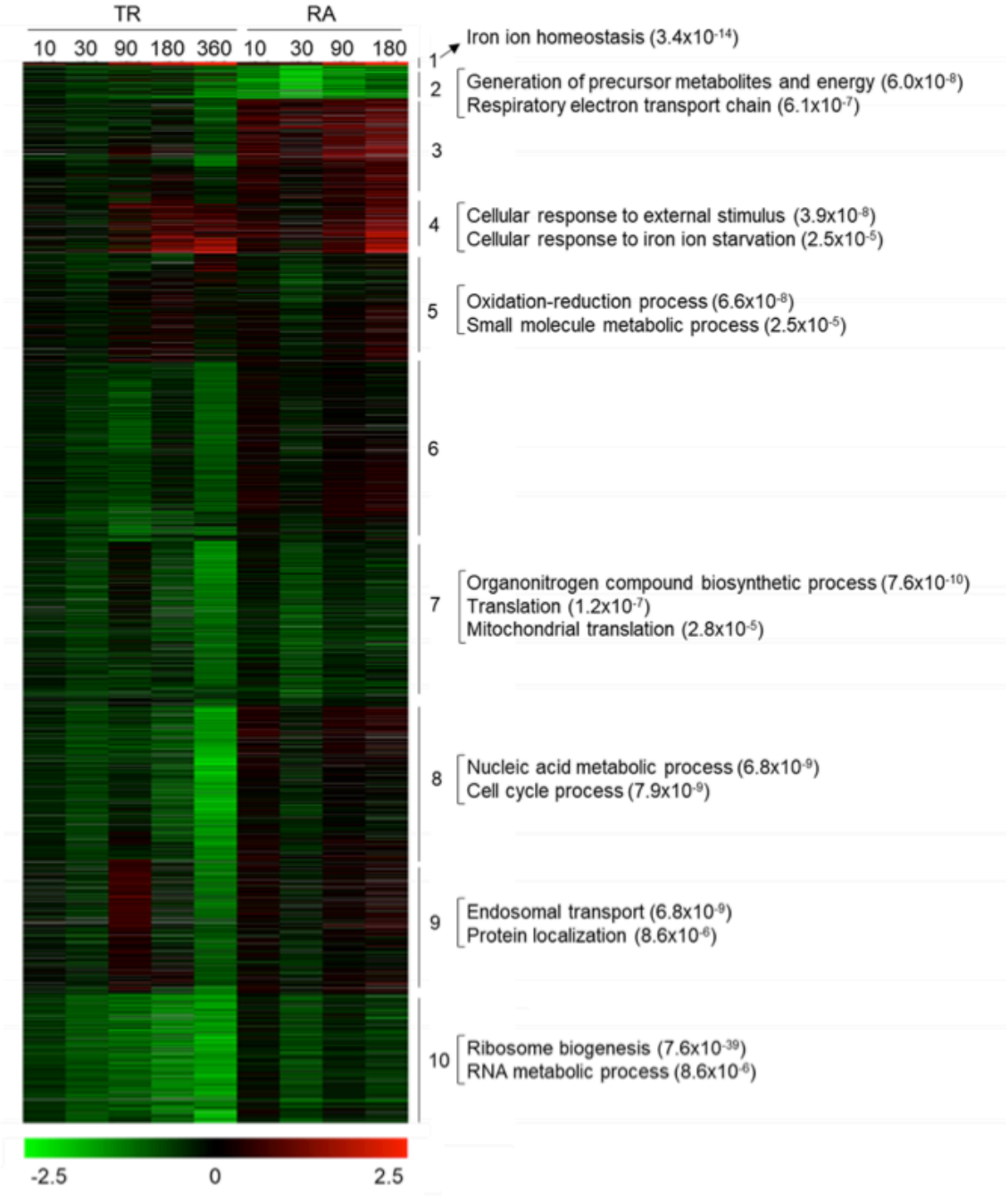

Figure 2. Clustering of genes according to their TR and RA profiles. Time course profiles for both parameters were considered for clustering. Dataset series are referred to their respective time zero in logarithm scale. Relative repression is shown in green and relative induction in red. The most significant GO categories (p value ≤ 10^{-4}) are indicated with their respective p values. The individual data for each gene and the list of genes in each cluster are listed in Supplementary Data S1 and S2, respectively.

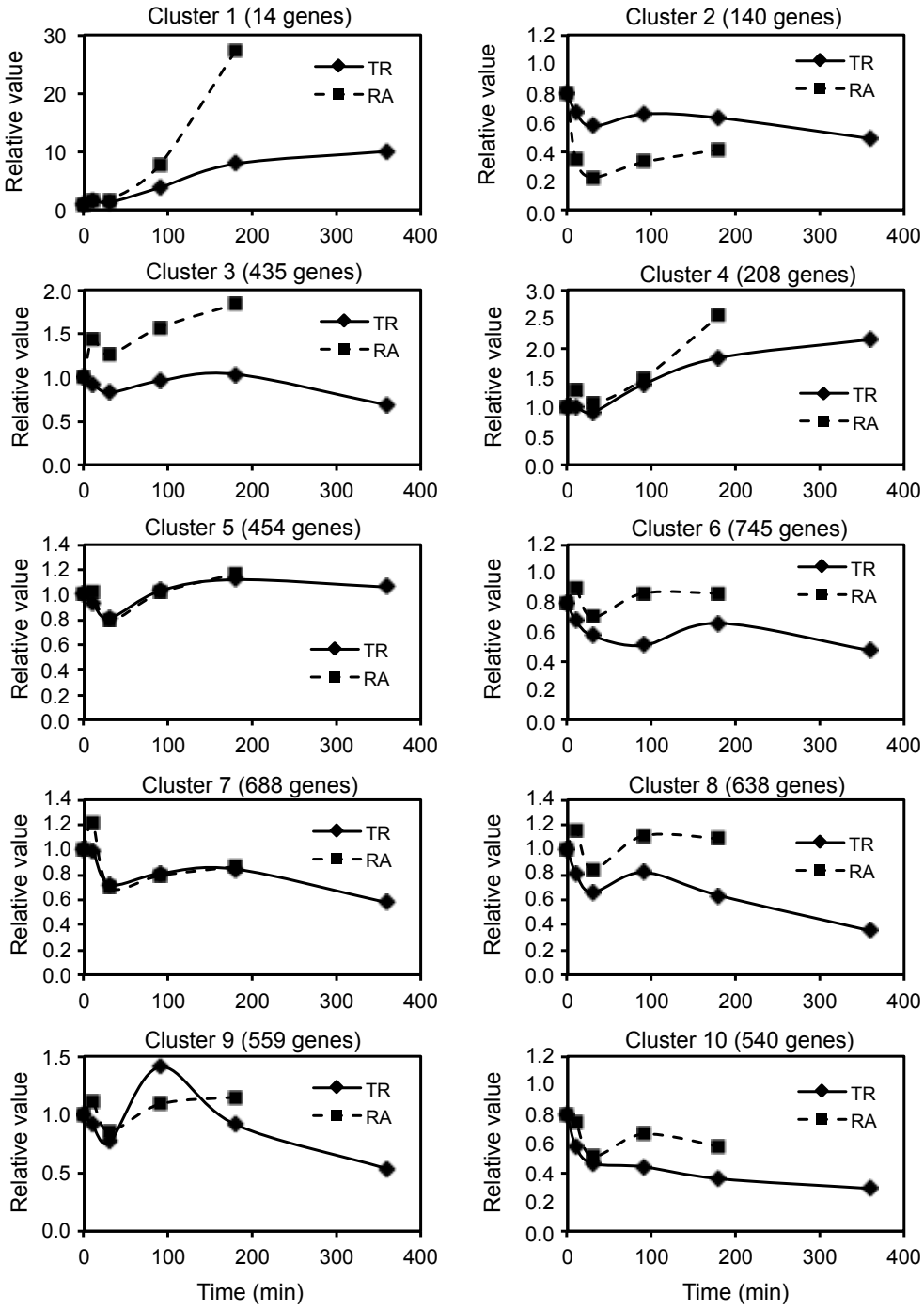

Figure 3. Global changes in TR and RA during the progress in iron deficiency corresponding to each cluster. The graphs represent the median TR and RA for all genes included in each group. The values are referred to time zero. Clusters are defined in Figure 2.

Previous studies have demonstrated that yeast cells initiate a common gene expression program called the environmental stress response (ESR) to acclimate to multiple suboptimal conditions [26-28]. The ESR set of genes is comprised of ~300 induced mRNAs (iESR), which encompass genes involved in protecting cells against stress conditions, and ~600 repressed transcripts (rESR) encoding RPs, RiBis and other proteins implicated in translation [26]. Since a notable conclusion of our clustering was the down-regulation of genes involved in ribosome biogenesis and translation ($p < 10^{-13}$), we decided to explore whether the ESR program was initiated in response to iron depletion. For this purpose, we represented the median TR and RA profiles of the iESR and rESR genes referred to a normalized global TR and RA pattern, respectively, during the progress of the iron limitation. Consistent with an activation of the ESR program, we observed an up-regulation of the iESR and a down-regulation of the rESR set of genes for both the TR and RA profiles in response to iron deficiency (Figure 4A). This result suggests that transcriptional mechanisms activate the ESR program upon iron depletion. To compare the ESR response initiated upon iron depletion to the one activated by other stresses [28], we represented the ESR genes described for the oxidative stress achieved by the addition of 0.1 mM *ter*-butyl hydroperoxide [29] (Figure 4A). The iron deficiency ESR response was milder and slower than the one commonly observed in response to oxidative and other stresses (Figure 4A, ESR RA-ox)[26, 28]. Previous studies had demonstrated that the general stress transcription factors Msn2 and Msn4 contribute to the activation of a set of the iESR genes in response to various stresses [26]. To ascertain the potential relevance of the iESR signature and the Msn2 and Msn4 transcription factors to the adaptation to iron depletion, we assayed the growth of an *msn2Δmsn4Δ* yeast

mutant in iron-deficient conditions and observed a significant decrease in growth as compared to wild-type cells (Figure 4B). These results support a role for the Msn2 and Msn4 transcription factors and the iESR genes in the response to iron deficiency.

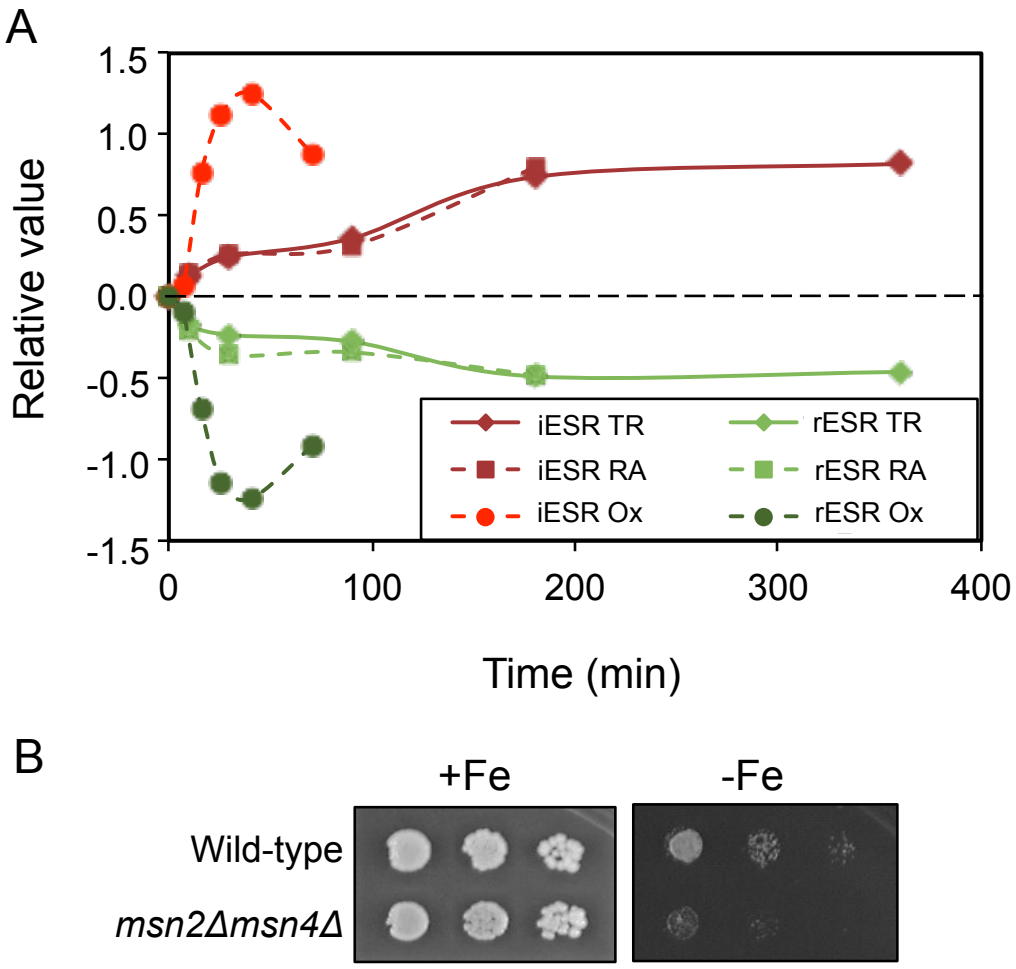

Figure 4. Activation of the ESR in response to iron depletion. (A) The median TR and RA corresponding to the genes classified as iESR and rESR was represented during the progress of the iron deficiency and referred to the normalized global patterns of TR and RA, respectively. The median RA pattern of the iESR and rESR genes in response to the oxidative stress achieved by addition of 0.1 mM *ter*-butyl hydroperoxide previously reported [29] is also represented as ESR-ox (circles). **(B)** Msn2 and Msn4 transcription factors are required for growth in iron-deficient conditions. Wild-type BY4741 and *msn2Δmsn4Δ* double mutant were grown in SC (+Fe) and SC with 600 μM Ferrozine (-Fe).

3.3. Iron limitation inhibits Sfp1 and the Sch9 branch of the TORC1 pathway

We noticed that the median TR of genes included in cluster 10, and specifically the RiBi and RP genes, decreased when the iron deficiency persisted (Figure 3; Supplementary Data S2). To verify that this drop in TR had a consequence in the RA, we determined the mRNA levels of specific RP and RiBi genes by RT-qPCR in two different yeast backgrounds, W303 and BY4741 (S288C). All the RP and RiBi genes tested diminished their RA during the progress of iron deficiency (Figures 5A, 5B and S2). Multiple pathways regulate the transcription of RP and RiBi genes. One of these mechanism involves the transcription factor Sfp1 that, in response to stress or low nutrient availability, exits the nucleus, and consequently RP and RiBi expression decreases (reviewed in [9]). We investigated Sfp1 subcellular localization under both iron-sufficient and deficient conditions. As expected, Sfp1 localized to the nucleus under iron-replete conditions (Figure 5C and 5D, left). Consistent with a decrease in RP and RiBi gene expression, Sfp1 exited the nucleus when iron was depleted (Figure 5C and 5D, right). These results demonstrate that Sfp1 subcellular localization responds to iron bioavailability, and probably alters RP and RiBi gene expression. Another mechanism that regulates RP and RiBi gene expression involves Stb3 and the paralog proteins Dot6 and Tod6, which recruit the RPD3L histone deacetylase complex to RP and RiBi promoters to repress transcription when growth conditions are not favorable [13]. Therefore, we determined the fold change of multiple RP and RiBi mRNAs in *dot6Δtod6Δ*, *stb3Δ*, and *rpd3Δ* mutants as compared to wild-type cells. The RA of the RP genes analyzed decreased in the iron-deficient wild-type strain, whereas no

decline was observed for the *stb3Δ* and *rpd3Δ* mutants (Figure 5E). Moreover, the RiBi RA down-regulation caused by iron depletion was disrupted in the *dot6Δtod6Δ* and *rpd3Δ* mutants (Figure 5F). These results strongly suggest that Stb3 and Dot6-Tod6 repress the expression of RP and RiBi genes respectively in response to iron deficiency, via the Rpd3 histone deacetylase.

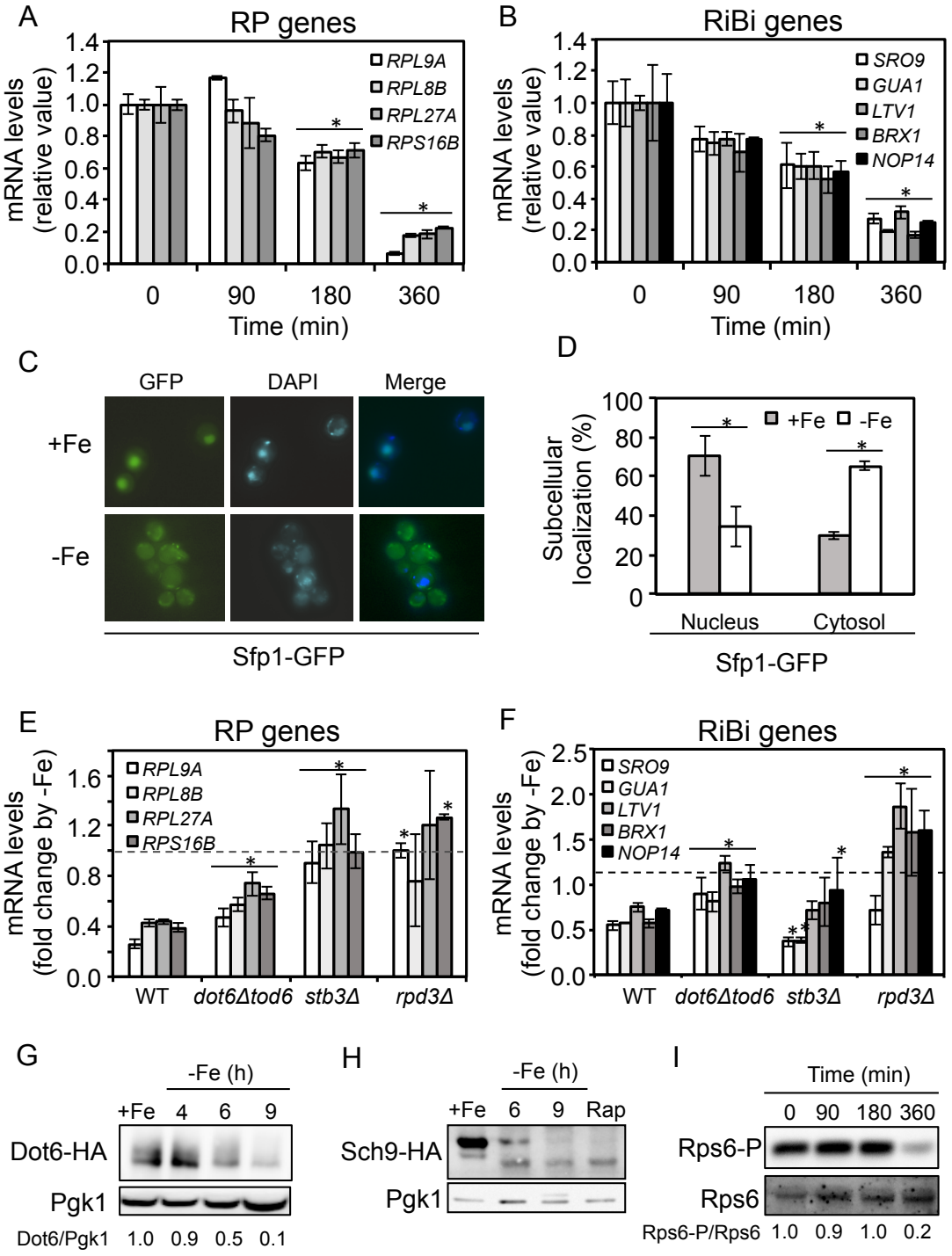

Figure 5. Regulation of Sfp1, Sch9, Dot6, Stb3, Rpd3, RP and RiBi genes in response to iron deficiency. (A, B) Determination of specific RP and RiBi mRNA levels during the progress of iron deficiency by RT-qPCR. W303 cells were grown as indicated in Figure 1A (GRO experiment). *ACT1* mRNA levels were used to normalize. Mean values and standard deviations from at least two independent experiments are

shown and referred to time zero. **(C, D)** Sfp1 relocalizes to the cytoplasm in response to iron deficiency. Wild type yeast cells transformed with the SFP1-GFP plasmid were grown at 30 °C in SD (+Fe) and SD with 100 μM BPS (-Fe) for 8 hours. Sfp1-GFP subcellular localization was determined by fluorescence microscopy. DAPI was used as a marker for the nucleus. A merge between GFP and DAPI is shown. Representative images are shown (panel C). The white bar represents 10 μm. The percentage of cells with either predominantly cytoplasmic or nuclear GFP signal was determined by triplicate. The average and the standard deviation are represented (Panel D). Similar results were obtained in SC. **(E, F)** Fold change in RP and RiBi mRNA levels. Wild type BY4741, *dot6Δtod6Δ*, *stb3Δ* y *rpd3Δ* yeast strains were grown at 30 °C in SC (+Fe) and SC with 100 μM BPS (-Fe) for 9 hours. Specific mRNA levels of RP and RiBi genes were determined as mentioned above. Mean values of fold induction in iron deficiency and standard deviations from at least two independent experiments are shown. **(G)** Dot6 protein levels. Yeast cells expressing *DOT6-HA* were grown at 30 °C in SC (+Fe) and SC with 100 μM BPS (-Fe) for 9 hours. Dot6-HA and Pgk1 protein levels were analyzed by western blot with anti-HA and anti-Pgk1 antibodies, respectively. Protein levels have been quantified and the Dot6-HA/Pgk1 ratio indicated. **(H)** Determination of Sch9 protein levels and phosphorylation state. Yeast cells expressing *SCH9-HA* were grown as in panel E and NTCB-treated protein extracts were analyzed as described in Materials and methods. **(I)** Determination of Rps6 protein levels and phosphorylation state. W303 cells were grown as described in Figure 1A. The levels of total Rps6 and phosphorylated Rps6 (Rps6-P) protein were determined by Western blot analyses using the anti-Rps6 and anti-Rps6-Ser235/236 antibodies, respectively. Protein levels have been quantified and the Rps6-P/Rps6 ratio indicated. A representative experiment of three independent biological replicates is shown.

Under optimal growth conditions, the TORC1 kinase complex directly phosphorylates and activates Sch9 kinase (reviewed in [9]). Then, Sch9 phosphorylates Stb3 and Dot6-Tod6 proteins, inhibiting their function and facilitating the transcription of RP and RiBi genes [13]. Upon TORC1 inhibition, Sch9 is dephosphorylated and deactivated, and accordingly the downstream Stb3

and Dot6-Tod6 proteins are also dephosphorylated and become active in the repression of RP and RiBi genes. The Stb3 and Dot6-Tod6 dependent down-regulation of RP and RiBi genes promoted by the depletion of iron predicted a dephosphorylation of these regulatory factors. We first observed that iron deficiency promoted a decrease in Dot6 protein abundance, although no convincing conclusions could be established on Dot6 phosphorylation state (Figure 5G and Figure S2C). Then, we determined the phosphorylation state of the key TORC1-dependent kinase Sch9. We observed that Sch9 protein was gradually dephosphorylated and its abundance diminished during the advance of the iron deficiency to reach a stage similar to that obtained with the rapamycin treatment (Figure 5H, Figure S2D and S2E). Collectively, these results suggest that the dephosphorylation of the TORC1-dependent kinase Sch9 limits the expression of RP and RiBi genes in response to iron starvation via Stb3, Dot6-Tod6 and Rpd3.

In addition to the regulation of RP and RiBi gene transcription, the inhibition of the TORC1 cascade promotes a decrease in the levels of newly synthesized ribosomal subunits that causes the nucleolar entrapment of specific ribosomal biogenesis factors [30]. To address if this was the case of iron deficiency, we determined the subcellular localization of the Rrp12-GFP protein, which is trapped in the nucleolus upon TOR inactivation [30]. We observed that the Rrp12-GFP protein did not properly distribute all over the cell when iron was scarce, but instead it was trapped in the nucleus (Figure S3). We also determined the phosphorylation state of the small ribosomal subunit Rps6, which is phosphorylated by the Ypk3 kinase in a TORC1-dependent manner [31, 32]. By using an antibody specific for its phosphorylated form, we could state that Rps6 dephosphorylates upon iron depletion, whereas no changes were observed for the

levels of total Rps6 protein (Figure 5I). Both Rrp12 mislocalization and Rps6 dephosphorylation support the inactivation of the TORC1 pathway by iron scarcity.

3.4. Iron starvation limits the transcription of all RNA polymerases

The TORC1 pathway coordinates the expression of RP and RiBi genes to rRNA and tRNA synthesis in response to different environmental conditions. Specifically, TORC1 regulates the activity of RNA Pol I, which is responsible for the transcription of the 35S precursor of the mature 25S, 18S and 5.8S rRNAs, and RNA Pol III, which transcribes tRNA genes and the 5S rRNA, at different steps in the transcription cycle (reviewed in [9]). Therefore, we explored whether the deprivation of iron altered the synthesis of rRNA. We first observed that the RA, which mostly corresponds to rRNA (~80%), was fairly constant up to three hours of iron deficiency, but lowered to 50% after 6 hours (Figure 6A). Consistent with a drop in the RA, we observed both a decrease in the RNA Pol I TR and a down-regulation of *25S* and *18S* RNA levels along the iron starvation period (Figures 6B and 6C). Different mechanisms could account for the decrease in RNA Pol I activity. We observed that the protein levels of the largest subunit of the RNA Pol I complex, A190 (Rpa190), strongly diminished after 6 hours of iron deficiency, when the decrease in RNA Pol I TR is more severe (Figures 6B and 6D). Furthermore, the abundance of the RNA Pol I activating protein Rrn3, which is degraded in response to TORC1 inactivation [12], decreased at severe iron deficiency (Figure 6E). These results demonstrate that the transcription of rRNAs by the RNA Pol I diminish in response to a prolonged iron deficiency.

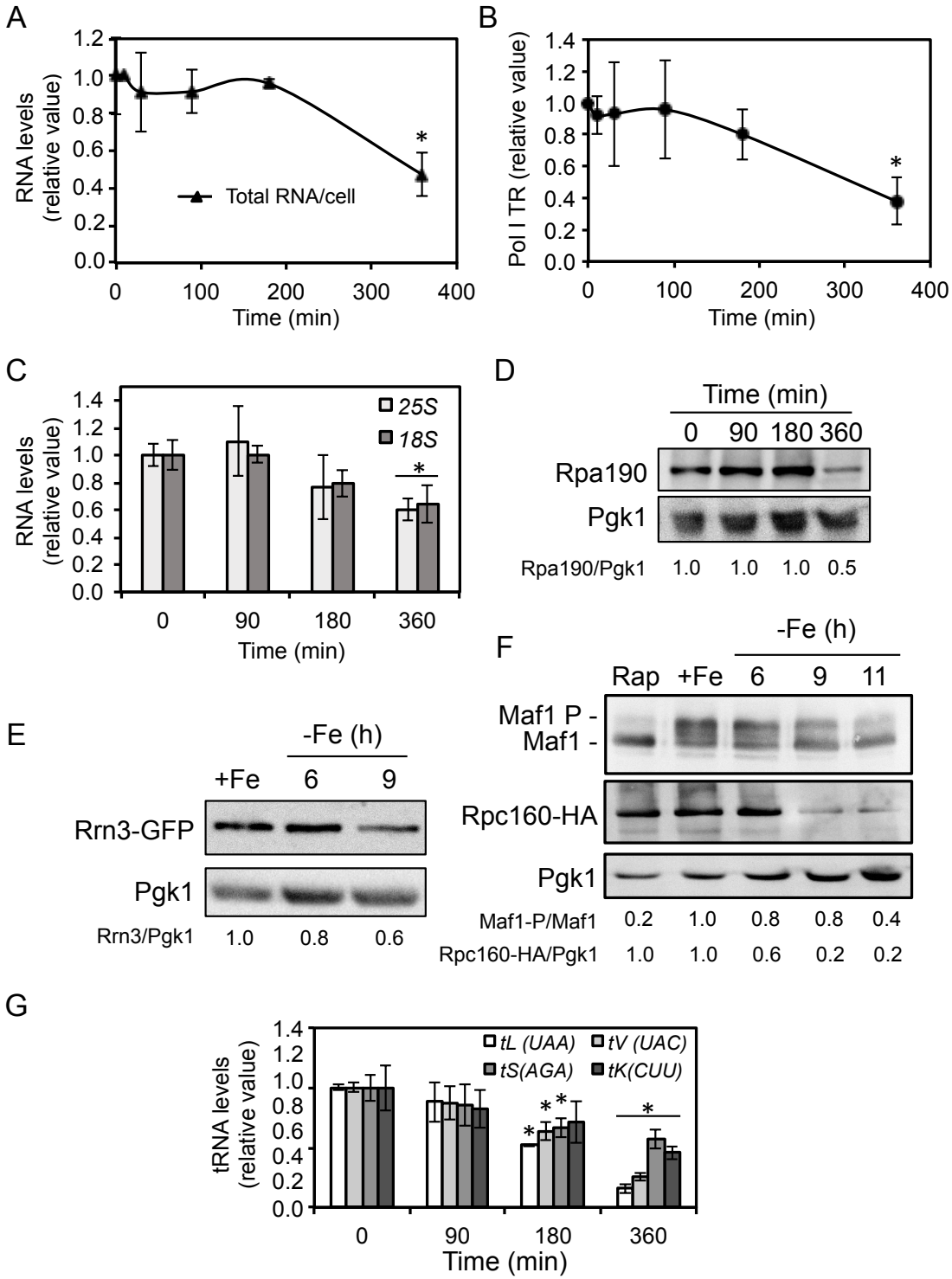

Figure 6. The activities of RNA polymerase I and III are inhibited in iron scarcity. **(A)** Total RNA per cell during the iron deficiency kinetics. W303 cells were grown as in Figure 1A and total RNA per cell determined. **(B)** The RNA Pol I transcription rate was determined by summing up the specific probes for *18S* and *25S* in every time point

of the GRO experiment. **(C)** The *18S* and *25S* RNA levels were analyzed by RT-qPCR using specific primers. *ACT1* was used to normalize. **(D)** The protein levels of the largest RNA Pol I subunit Rpa190 and Pgk1 were determined by Western Blot using the anti-Rpa190 and anti-Pgk1 antibodies, respectively. **(E)** Determination of Rrn3 protein levels. Yeast cells expressing *RRN3-GFP* were grown at 30 °C in SC (+Fe) and SC with 100 µM BPS (-Fe) for 9 hours. Rrn3-GFP and Pgk1 protein levels were analyzed with anti-GFP and anti-Pgk1 antibodies, respectively. **(F)** Yeast cells expressing HA epitope-tagged RPC160 were grown at 30 °C in SC (+Fe), SC with 100 µM BPS (-Fe) for 11 hours and in presence of rapamycin (200 ng/ml) for 30 minutes. Rpc160-HA, Maf1 and Pgk1 protein levels were analyzed by Western blot with anti-HA, anti-Maf1 and anti-Pgk1 antibodies, respectively. Rpa190, Rrn3-GFP, Maf1, RPC160-HA, and Pgk1 protein levels have been quantified, and the Rpa190/Pgk1, Rrn3/Pgk1, Rpc160-HA/Pgk1 and Maf1-P (phosphorylated)/Maf1 ratio indicated. **(G)** Determination of specific tRNA levels. The level of some tRNAs was determined in the same conditions as mentioned to develop the GRO by RT-qPCR using specific primers. *ACT1* was used to normalize.

The TORC1-dependent kinase Sch9 also regulates the RNA Pol III inhibitor protein Maf1. Under conditions favorable for growth, Sch9 phosphorylates Maf1, leading to its retention in the cytoplasm. On the contrary, TORC1 inactivation leads to the dephosphorylation of Maf1 and its accumulation in the nucleus where it binds to the RNA Pol III blocking tRNA synthesis [22]. To investigate whether this branch of the TORC1 pathway was also altered by changes in iron availability, we determined the electrophoretic mobility of Maf1 protein under iron-deficient conditions, which is an indicative of its phosphorylation state. Similarly to the rapamycin treatment, the depletion of iron led to the loss of Maf1 upper band corresponding to its phosphorylated form (Figure 6F and S4). Moreover, as shown for the biggest subunit of RNA Pol I and II (Figures 1B and 6D), the protein levels of the largest RNA Pol III subunit C160 (Rpc160-HA) also diminished in response to

low iron levels (Figure 6F). Consistent with defects in RNA Pol III activity, the levels of multiple tRNAs decreased in iron-deficient conditions (Figure 6G). The decrease in total and elongating RNA Pol II shown above (Figure 1C) matches with the pattern exhibited by the other two RNA Pol (Figure 6D and 6F). Thus, these results strongly suggest that the activity of all RNA polymerases decreases in response to iron deficiency via TORC1-dependent and probably independent mechanisms.

3.5. Iron deficiency activates the mitochondrial retrograde pathway

The Lst8 integral component of the TORC1 kinase complex negatively regulates the mitochondrial RTG pathway. Therefore, TORC1 inhibition activates the RTG signaling. To address whether this was the case in iron deficiency, we paid attention to the TR of the RTG genes *IDH1*, *IDH2*, and *CIT2* , which were included in the TR+RA cluster 4. Remarkably, the TR of all RTG genes augmented at severe iron depletion (Figure 7A). This TR up-regulation correlated with an increase in mRNA levels, except for the *ACO1* transcript (Figure 7B). Previous studies had shown that, in response to iron depletion, the mRNA-binding proteins Cth1 and Cth2 promote the degradation of multiple mRNAs including *ACO1* [16, 33]. Consistent with a simultaneous post-transcriptional decay by Cth1 and Cth2, we observed an increase in *ACO1* mRNA levels in iron-deficient *cth1Δcth2Δ* cells (Figure S5A). The Rtg1-Rtg3 transcription factors and the Rtg2 regulatory protein activate the RTG pathway in response to mitochondrial defects [14, 15]. Various observations indicated that they were also required for the activation of the RTG pathway when iron was scarce. First, no up-regulation in the mRNA levels of the

different *RTG* genes was observed in iron-deficient *rtg1Δ*, *rtg2Δ* and *rtg3Δ* cells (Figure 7C). Second, a fusion of the *ACO1* promoter to *lacZ* caused an increase in β-galactosidase activity when iron was depleted, which did not occur in *rtg1Δ*, *rtg2Δ* and *rtg3Δ* cells (Figure S5B). Third, RNA Pol II was recruited to the promoter of *RTG* genes in response to iron depletion in wild-type cells but not in *rtg1Δ* mutants (Figure 7D). And fourth, Rtg1 transcription factor moved to the nucleus upon iron deficiency (Figure 7E and 7F). Taken together, these results demonstrate that the mitochondrial RTG response is activated in response to iron depletion.

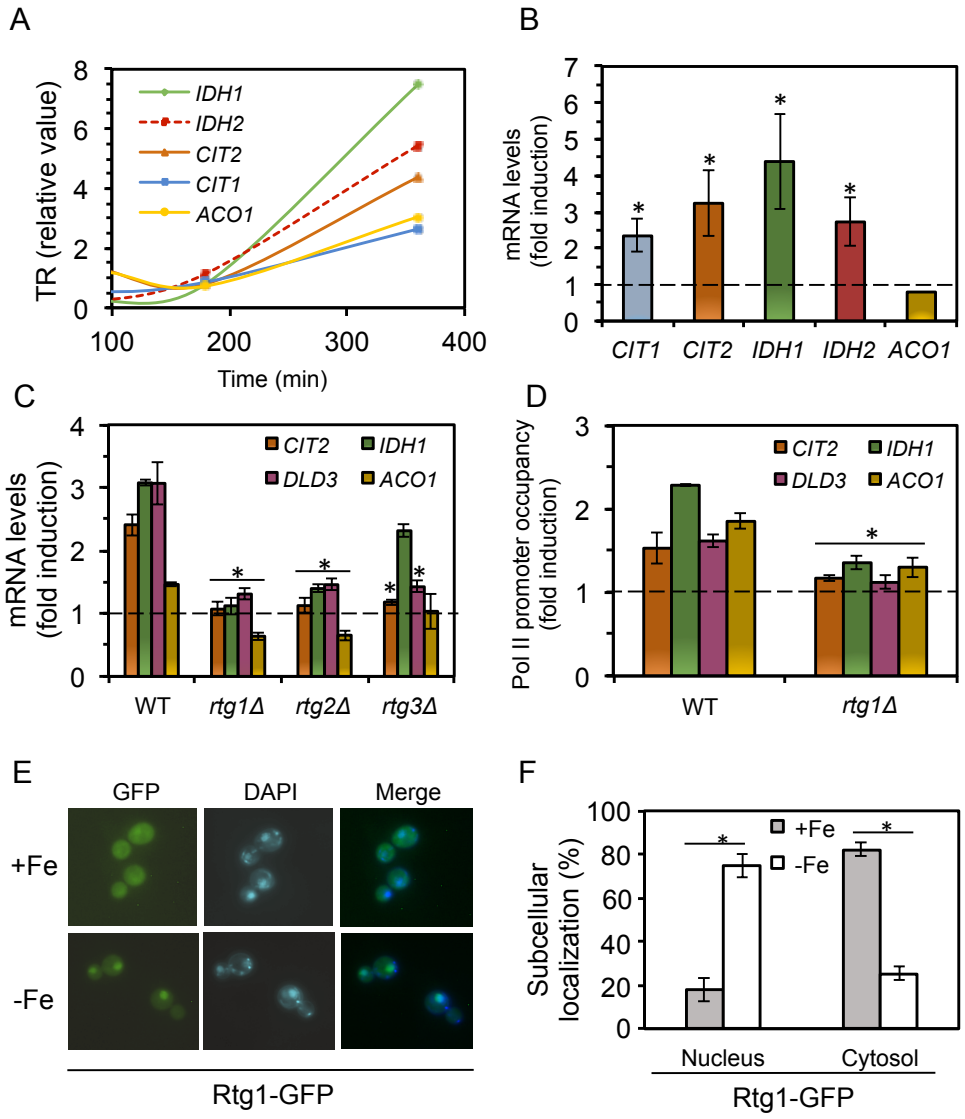

Figure 7. The retrograde pathway is transcriptionally activated upon iron depletion. (A) Transcription rates of *RTG* genes during the response to iron deficiency obtained from the GRO experiment. **(B)** Fold induction of *RTG* mRNA levels in response to low iron. W303 cells were grown as described in Figure 1A, and RNA extracted and analyzed at six hours of iron deficiency by RT-qPCR using specific primers. **(C)** Wild type BY4741, *rtg1Δ, rtg2Δ and rtg3Δ* strains were grown at 30 °C in SC (+Fe) and SC with 100 μM BPS (-Fe) for 9 hours. The mRNA levels of specific *RTG* genes were determined by RT-qPCR using specific primers. *ACT1* was used as a loading control. Mean values of fold induction in iron deficiency and standard deviations from at least two independent experiments are shown. **(D)** RNA Pol II chromatin immunoprecipitation. The wild-type BY4741 and *rtg1Δ* cells were grown as described in panel B. Proteins were extracted and immunoprecipitated with anti-RNA Pol II monoclonal antibody. DNA was extracted and binding to *RTG* promoter regions was determined by RT-qPCR. The results were normalized to *FUS1* promoter. Mean values of fold induction in iron deficiency and standard deviations from at least two independent experiments are shown. **(E, F)** Rtg1 moves to the nucleus in response to iron deficiency. Wild type yeast cells transformed with the RTG1-GFP plasmid were grown at 30 °C in SD (+Fe) and SD with 100 μM BPS (-Fe) for 8 hours. Rtg1-GFP subcellular localization was determined by fluorescence microscopy. DAPI was used as a marker for the nucleus. A merge between GFP and DAPI is shown Representative images are shown (panel E). The white bar represents 10 μm. The percentage of cells with either predominantly cytoplasmic or nuclear GFP signal was determined by triplicate. The average and the standard deviation are represented (Panel F). Similar results were obtained in SC.

4. Discussion

Gene expression studies on the yeast *S. cerevisiae* have focused on the alterations in steady-state mRNA levels that occur when iron is scarce. However, regardless of Aft1-Aft2 mediated regulation, few studies have assessed the contribution of changes in the TR to the response to low iron conditions [34]. Similarly to other stresses [26, 28], iron depletion activates the yeast ESR program including the up-regulation of stress-related genes and the down-regulation of genes implicated in protein translation (Figure 4). The analysis of both RA and TR profiles for the ESR also suggests that this regulation is mainly exerted at the level of transcription probably via Msn2/Msn4 for the iESR, and Sfp1, Dot6-Tod6 and Stb3 for the rESR. A recent study has demonstrated that the initiation of the ESR is not simply the consequence of changes in the growth rate or the cell-cycle phase [27]. Instead, failure to down-regulate the rESR genes leads to a defect in polysome association and translation of the iESR transcripts [27]. These data strongly suggest that yeast stressed cells redirect its translational capacity toward the synthesis of the induced transcripts [27], which in the case of iron depletion would presumably include the machinery for iron uptake and mobilization, the RTG response, and some stress-related genes such as Ole1 fatty acid desaturase. An important difference between the ESR signature observed in response to multiple non-lethal stresses and the profile observed in response to iron deficiency is that in the former case the ESR response is faster but transient [26, 28], probably due to cells benefit from going back to non-stress transcriptome after having solved the molecular hazards, whereas iron deficiency, which is a nutritional defect, is irreversible and the ESR remains activated at intermediate levels unless iron bioavailability resumes (Figure 3A).

Despite the global decrease in TR that occurs in response to iron limitation, yeast cells remarkably activate the transcription of genes from the mitochondrial RTG via the Rtg1/Rtg3 and Rtg2 regulatory factors (Figure 7). The physiological significance of RTG activation by iron depletion could be to ensure the supply of sufficient α-ketoglutarate, which is the source of glutamate, required as a nitrogen donor for biosynthetic processes. This is especially important under iron-deficient conditions because the iron-requiring pathway for glutamate synthesis that depends on the iron sulfur cluster-containing enzyme glutamate synthase Glt1 is repressed, and all glutamate biosynthesis relies on glutamate dehydrogenases Gdh1 and Gdh3 [17]. Several factors could contribute to the initiation of the mitochondrial RTG signaling in response to iron depletion. Iron deficiency limits the expression of multiple components of the TCA cycle and the electron transport chain, which compromises mitochondrial respiration and eventually could decrease ATP concentration and mitochondrial membrane potential, which is a signal to activate the retrograde response [35]. Therefore, mitochondrial malfunctions would be the main candidate to trigger RTG activation when iron is scarce. However, other factors could participate in this regulation. For instance, the E3 ubiquitin ligase complex SCF^{Grr1}, which positively regulates RTG signaling by promoting the ubiquitination and degradation of the Rtg1/Rtg3-inhibitor protein Mks1, has been recently implicated in the degradation of the iron-regulated protein Cth2, and *grr1Δ* cells are unable to grow in iron-deficient conditions [36]. Importantly, the integral component of the TORC1 complex Lst8 negatively regulates the RTG signaling pathway acting both upstream and downstream of Rtg2 (reviewed in [14, 15]). The connection between the RTG and the TORC1

kinase pathway is bidirectional, since mitochondrial dysfunctions also lead to a decrease in the phosphorylation state and activity of the Sch9 kinase [37].

Studies in different organisms have suggested that TOR signaling influences iron metabolism (reviewed in [38]). We showed that mammalian TOR (mTOR) modulates the expression of iron transporters and the cellular flux of iron via tristetraprolin, the mammalian Cth2 homologue [39]. Consistent with this, it has been shown that the disturbance of the mTORC1 pathway in red blood cells resulted in anemia [40]. A proteomic study reported that TOR gene silencing deregulates the import of proteins into the mitochondria and the adaptation to iron starvation of the human pathogenic fungus *Aspergillus fumigatus* [41]. In yeast, the inhibition of TOR pathway by Torin2, a potent inhibitor of both TORC1 and TORC2 has been recently shown to increase the expression of metalloreductases involved in iron uptake leading to excess iron sensitivity [42]. The influence of cellular and systemic iron status on mTOR signaling has also been explored [38]. To this end, the expression or phosphorylation status of either the mTOR kinase, its upstream regulators Akt, TSC2 or REDD1, or its downstream target ribosomal protein S6, have been determined. However, the conclusions drawn with these studies are contradictory. On one side, data with iron-deficient rats, murine red blood cells, human myeloid leukemia and intestinal epithelia cells suggest that iron depletion could inactivate mTOR signaling [40, 43-45]. On the other side, two genetic mouse models that cause neuronal-specific iron deficiency support the opposite conclusion [46]. TORC1 studies in yeast have enormously increased our current understanding of the contribution of this pathway to nutrient signaling and growth control [9, 10]. By using a yeast genome-wide approach, we have shown here that iron deficiency inhibits protein synthesis via

the TORC1 pathway. Multiple specific molecular markers including Sch9, Maf1 and Rps6 dephosphorylation, nuclear retention of Rrp12, and decreased expression of RP, RiBi, rRNA and tRNA genes are consistent with TORC1 inhibition when iron bioavailability decreases (Figure 8).

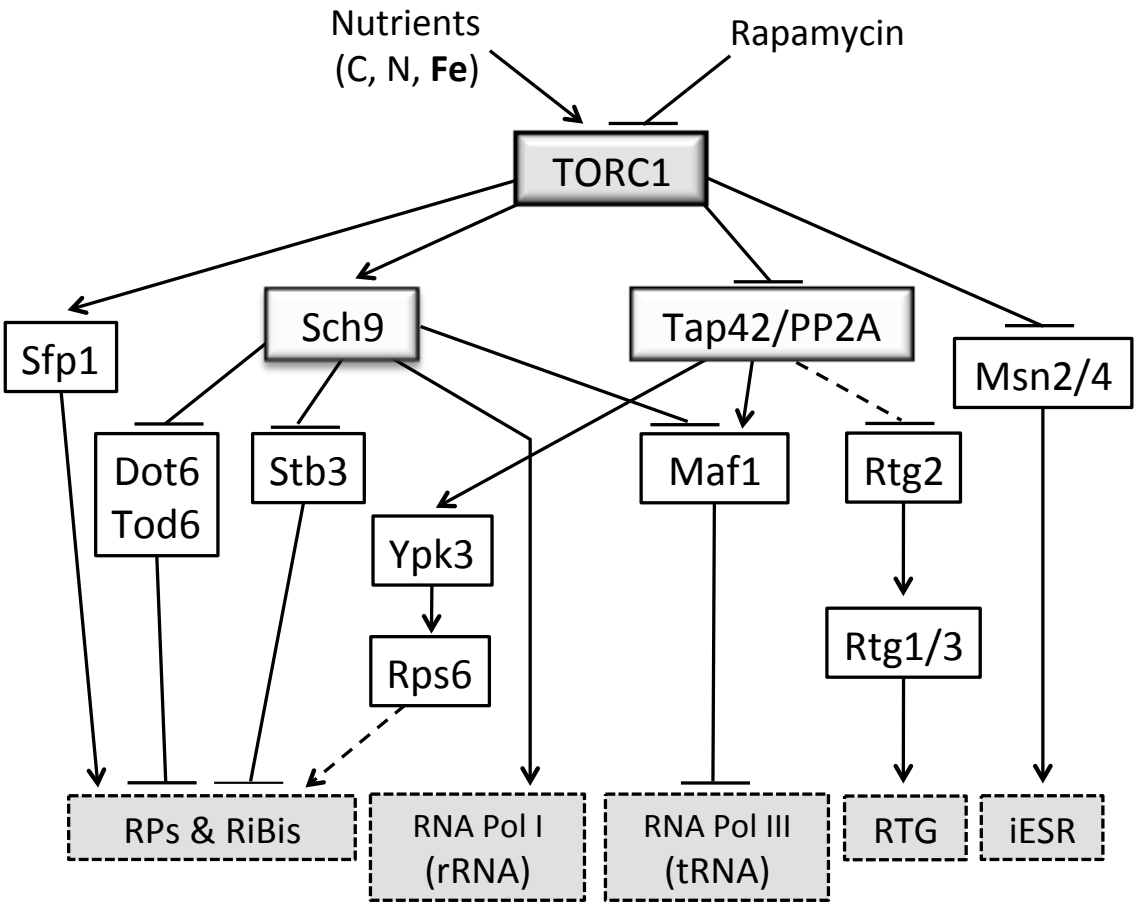

Figure 8. A model for TORC1 regulation in response to iron depletion. Upon iron deficiency, yeast cells inhibit the TORC1 pathway. Consequently, yeast represses the transcription of RP and RiBi genes, and the activity of the RNA Pol I and III. Moreover, the ESR pathway is transcriptionally activated in response to iron scarcity. Multiple effectors of the TORC1 pathway including the Sch9 kinase, Maf1, Rps6 and the transcription factors Sfp1, Dot6 and Msn2/Msn4 are regulated by iron bioavailability.

TORC1 constitutes a major hub to sense and respond to nutrients, in particular to amino acid and glucose levels [23]. The alteration of cellular and

systemic iron homeostasis is on the basis of microbial pathogenesis and many disorders including chronic anemia, hemochromatosis, thalassemia, aceruloplasminemia, various neurodegenerative diseases and cancer [47]; whereas TORC1 has been implicated in fungal virulence, aging, cancer, cardiovascular diseases, and autoimmune and metabolic disorders such as diabetes and obesity [9, 11, 48]. A better comprehension of the crosstalk between eukaryotic iron metabolism, TOR signaling and microbial virulence is necessary to understand the impact of current treatments and to develop novel therapeutic strategies for both iron and TOR related diseases in a selective manner.

5. Acknowledgements

We thank the members of the "Iron Homeostasis" and "Yeast Functional Genomics" laboratories for scientific comments and technical assistance, especially Dr. Paula Alepuz, Dr. Daniel Medina, and Pilar Miró. We are also grateful to Drs. Emilia Matallana, Olga Calvo, Francisco Navarro, Francisco Estruch, John Zaborske, Olivier Lefebvre, Fred Cross, Andrew Capaldi, Joachim Griesenbeck, Charles Moehle, and Ted Powers for providing yeast strains, plasmids or antibodies used in this study.

This work was supported by predoctoral contracts from the Spanish Ministry of Science, Innovation and Universities (MICINN) to AMR and LRA; a fellowship from the "Generalitat de Catalunya" (Spain) to SMM; European Union Funds (FEDER) and MICINN grants BIO2017-87828-C2-1-P to SP, BIO2017-87828-C2-2-P to MATR, BFU2016-77728-C3-3-P to JEPO, and BFU2015-71978-REDT to

SP and JEPO; and Regional Government of Valencia PROMETEOII 2015/006 grant to JEPO.

6. Author contributions

Antonia M. Romero: Investigation, Writing – review and editing, visualization; Analysis and interpretation of data. Lucia Ramos-Alonso: Investigation, Writing – review and editing. Sandra Montellá-Manuel: Investigation. José García-Martínez: Writing – review and editing, Analysis and interpretation of data. María Ángeles de la Torre-Ruiz: Investigation, Funding acquisition, Analysis and interpretation of data. José E. Pérez-Ortín: Resources, Writing – review and editing, Funding acquisition, Analysis and interpretation of data. María T. Martínez-Pastor: Conceptualization, Writing - original draft, Project administration. Sergi Puig: Conceptualization, Resources, Writing - original draft, Funding acquisition, Project administration, visualization.

7. References

[1] M.B. Zimmermann, R.F. Hurrell, Nutritional iron deficiency, Lancet, 370 (2007) 511-520.
[2] W.H. Jung, J.W. Kronstad, Iron and fungal pathogenesis: a case study with Cryptococcus neoformans, Cell Microbiol, 10 (2008) 277-284.
[3] R.S. Almeida, D. Wilson, B. Hube, Candida albicans iron acquisition within the host, FEMS Yeast Res, 9 (2009) 1000-1012.
[4] F. Gerwien, V. Skrahina, L. Kasper, B. Hube, S. Brunke, Metals in fungal virulence, FEMS Microbiol Rev, 42 (2018).
[5] C.C. Philpott, O. Protchenko, Response to iron deprivation in Saccharomyces cerevisiae, Eukaryot Cell, 7 (2008) 20-27.
[6] C.D. Kaplan, J. Kaplan, Iron acquisition and transcriptional regulation, Chem Rev, 109 (2009) 4536-4552.
[7] N. Sanvisens, S. Puig, Causes and consequences of nutritional iron deficiency in living organisms, in: T.C. Merkin (Ed.) Biology of starvation in humans and other organisms, Nova Science Publishers, Place Published, 2011, pp. 245-276.

[8] J.C. Rutherford, A.J. Bird, Metal-responsive transcription factors that regulate iron, zinc, and copper homeostasis in eukaryotic cells, Eukaryot Cell, 3 (2004) 1-13.
[9] R. Loewith, M.N. Hall, Target of rapamycin (TOR) in nutrient signaling and growth control, Genetics, 189 (2011) 1177-1201.
[10] A. Gonzalez, M.N. Hall, Nutrient sensing and TOR signaling in yeast and mammals, EMBO J, 36 (2017) 397-408.
[11] S. Wullschleger, R. Loewith, M.N. Hall, TOR signaling in growth and metabolism, Cell, 124 (2006) 471-484.
[12] A. Philippi, R. Steinbauer, A. Reiter, S. Fath, I. Leger-Silvestre, P. Milkereit, J. Griesenbeck, H. Tschochner, TOR-dependent reduction in the expression level of Rrn3p lowers the activity of the yeast RNA Pol I machinery, but does not account for the strong inhibition of rRNA production, Nucleic Acids Res, 38 (2010) 5315-5326.
[13] A. Huber, S.L. French, H. Tekotte, S. Yerlikaya, M. Stahl, M.P. Perepelkina, M. Tyers, J. Rougemont, A.L. Beyer, R. Loewith, Sch9 regulates ribosome biogenesis via Stb3, Dot6 and Tod6 and the histone deacetylase complex RPD3L, EMBO J, 30 (2011) 3052-3064.
[14] S.M. Jazwinski, The retrograde response: a conserved compensatory reaction to damage from within and from without, Prog Mol Biol Transl Sci, 127 (2014) 133-154.
[15] Z. Liu, R.A. Butow, Mitochondrial retrograde signaling, Annu Rev Genet, 40 (2006) 159-185.
[16] S. Puig, E. Askeland, D.J. Thiele, Coordinated remodeling of cellular metabolism during iron deficiency through targeted mRNA degradation, Cell, 120 (2005) 99-110.
[17] M. Shakoury-Elizeh, J. Tiedeman, J. Rashford, T. Ferea, J. Demeter, E. Garcia, R. Rolfes, P.O. Brown, D. Botstein, C.C. Philpott, Transcriptional remodeling in response to iron deprivation in Saccharomyces cerevisiae, Mol Biol Cell, 15 (2004) 1233-1243.
[18] A. Hausmann, B. Samans, R. Lill, U. Muhlenhoff, Cellular and mitochondrial remodeling upon defects in iron-sulfur protein biogenesis, J Biol Chem, 283 (2008) 8318-8330.
[19] J. Garcia-Martinez, A. Aranda, J.E. Perez-Ortin, Genomic run-on evaluates transcription rates for all yeast genes and identifies gene regulatory mechanisms, Mol Cell, 15 (2004) 303-313.
[20] L. Ramos-Alonso, A.M. Romero, M.A. Soler, A. Perea-Garcia, P. Alepuz, S. Puig, M.T. Martinez-Pastor, Yeast Cth2 protein represses the translation of ARE-containing mRNAs in response to iron deficiency, PLoS Genet, 14 (2018) e1007476.
[21] J. Urban, A. Soulard, A. Huber, S. Lippman, D. Mukhopadhyay, O. Deloche, V. Wanke, D. Anrather, G. Ammerer, H. Riezman, J.R. Broach, C. De Virgilio, M.N. Hall, R. Loewith, Sch9 is a major target of TORC1 in Saccharomyces cerevisiae, Mol Cell, 26 (2007) 663-674.
[22] D. Oficjalska-Pham, O. Harismendy, W.J. Smagowicz, A. Gonzalez de Peredo, M. Boguta, A. Sentenac, O. Lefebvre, General repression of RNA polymerase III transcription is triggered by protein phosphatase type 2A-mediated dephosphorylation of Maf1, Mol Cell, 22 (2006) 623-632.

[23] J.E. Hughes Hallett, X. Luo, A.P. Capaldi, State transitions in the TORC1 signaling pathway and information processing in Saccharomyces cerevisiae, Genetics, 198 (2014) 773-786.
[24] A.M. Romero, T. Jorda, N. Rozes, M.T. Martinez-Pastor, S. Puig, Regulation of yeast fatty acid desaturase in response to iron deficiency, Biochim Biophys Acta Mol Cell Biol Lipids, 1863 (2018) 657-668.
[25] C.A. Martinez-Garay, R. de Llanos, A.M. Romero, M.T. Martinez-Pastor, S. Puig, Responses of Saccharomyces cerevisiae Strains from Different Origins to Elevated Iron Concentrations, Appl Environ Microbiol, 82 (2016) 1906-1916.
[26] A.P. Gasch, P.T. Spellman, C.M. Kao, O. Carmel-Harel, M.B. Eisen, G. Storz, D. Botstein, P.O. Brown, Genomic expression programs in the response of yeast cells to environmental changes, Mol Biol Cell, 11 (2000) 4241-4257.
[27] Y.H. Ho, E. Shishkova, J. Hose, J.J. Coon, A.P. Gasch, Decoupling Yeast Cell Division and Stress Defense Implicates mRNA Repression in Translational Reallocation during Stress, Curr Biol, 28 (2018) 2673-2680 e2674.
[28] D. Canadell, J. Garcia-Martinez, P. Alepuz, J.E. Perez-Ortin, J. Arino, Impact of high pH stress on yeast gene expression: A comprehensive analysis of mRNA turnover during stress responses, Biochim Biophys Acta, 1849 (2015) 653-664.
[29] M.M. Molina-Navarro, L. Castells-Roca, G. Belli, J. Garcia-Martinez, J. Marin-Navarro, J. Moreno, J.E. Perez-Ortin, E. Herrero, Comprehensive transcriptional analysis of the oxidative response in yeast, J Biol Chem, 283 (2008) 17908-17918.
[30] A. Reiter, R. Steinbauer, A. Philippi, J. Gerber, H. Tschochner, P. Milkereit, J. Griesenbeck, Reduction in ribosomal protein synthesis is sufficient to explain major effects on ribosome production after short-term TOR inactivation in Saccharomyces cerevisiae, Mol Cell Biol, 31 (2011) 803-817.
[31] S. Yerlikaya, M. Meusburger, R. Kumari, A. Huber, D. Anrather, M. Costanzo, C. Boone, G. Ammerer, P.V. Baranov, R. Loewith, TORC1 and TORC2 work together to regulate ribosomal protein S6 phosphorylation in Saccharomyces cerevisiae, Mol Biol Cell, 27 (2016) 397-409.
[32] A. Gonzalez, M. Shimobayashi, T. Eisenberg, D.A. Merle, T. Pendl, M.N. Hall, T. Moustafa, TORC1 promotes phosphorylation of ribosomal protein S6 via the AGC kinase Ypk3 in Saccharomyces cerevisiae, PLoS One, 10 (2015) e0120250.
[33] S. Puig, S.V. Vergara, D.J. Thiele, Cooperation of two mRNA-binding proteins drives metabolic adaptation to iron deficiency, Cell Metab, 7 (2008) 555-564.
[34] J. Ihrig, A. Hausmann, A. Hain, N. Richter, I. Hamza, R. Lill, U. Muhlenhoff, Iron regulation through the back door: iron-dependent metabolite levels contribute to transcriptional adaptation to iron deprivation in *Saccharomyces cerevisiae*, Eukaryot Cell, 9 (2010) 460-471.
[35] M.V. Miceli, J.C. Jiang, A. Tiwari, J.F. Rodriguez-Quinones, S.M. Jazwinski, Loss of mitochondrial membrane potential triggers the retrograde response extending yeast replicative lifespan, Front Genet, 2 (2011) 102.
[36] A.M. Romero, M. Martinez-Pastor, G. Du, C. Sole, M. Carlos, S.V. Vergara, N. Sanvisens, J.A. Wohlschlegel, D.P. Toczyski, F. Posas, E. de Nadal, M.T. Martinez-Pastor, D.J. Thiele, S. Puig, Phosphorylation and Proteasome Recognition of the mRNA-Binding Protein Cth2 Facilitates Yeast Adaptation to Iron Deficiency, MBio, 9 (2018).
[37] S. Kawai, J. Urban, M. Piccolis, N. Panchaud, C. De Virgilio, R. Loewith, Mitochondrial genomic dysfunction causes dephosphorylation of Sch9 in the yeast Saccharomyces cerevisiae, Eukaryot Cell, 10 (2011) 1367-1369.

[38] P. Guan, N. Wang, Mammalian target of rapamycin coordinates iron metabolism with iron-sulfur cluster assembly enzyme and tristetraprolin, Nutrition, 30 (2014) 968-974.
[39] M. Bayeva, A. Khechaduri, S. Puig, H.C. Chang, S. Patial, P.J. Blackshear, H. Ardehali, mTOR regulates cellular iron homeostasis through tristetraprolin, Cell Metab, 16 (2012) 645-657.
[40] Z.A. Knight, S.F. Schmidt, K. Birsoy, K. Tan, J.M. Friedman, A critical role for mTORC1 in erythropoiesis and anemia, Elife, 3 (2014) e01913.
[41] C. Baldin, V. Valiante, T. Kruger, L. Schafferer, H. Haas, O. Kniemeyer, A.A. Brakhage, Comparative proteomics of a tor inducible Aspergillus fumigatus mutant reveals involvement of the Tor kinase in iron regulation, Proteomics, 15 (2015) 2230-2243.
[42] P. Kumar, A. Awasthi, V. Nain, B. Issac, R. Puria, Novel insights into TOR signalling in Saccharomyces cerevisiae through Torin2, Gene, 669 (2018) 15-27.
[43] J.H. Ohyashiki, C. Kobayashi, R. Hamamura, S. Okabe, T. Tauchi, K. Ohyashiki, The oral iron chelator deferasirox represses signaling through the mTOR in myeloid leukemia cells by enhancing expression of REDD1, Cancer Sci, 100 (2009) 970-977.
[44] M. Ndong, M. Kazami, T. Suzuki, M. Uehara, S. Katsumata, H. Inoue, K. Kobayashi, T. Tadokoro, K. Suzuki, Y. Yamamoto, Iron deficiency down-regulates the Akt/TSC1-TSC2/mammalian Target of Rapamycin signaling pathway in rats and in COS-1 cells, Nutr Res, 29 (2009) 640-647.
[45] A. Watson, C. Lipina, H.J. McArdle, P.M. Taylor, H.S. Hundal, Iron depletion suppresses mTORC1-directed signalling in intestinal Caco-2 cells via induction of REDD1, Cell Signal, 28 (2016) 412-424.
[46] S.J. Fretham, E.S. Carlson, M.K. Georgieff, Neuronal-specific iron deficiency dysregulates mammalian target of rapamycin signaling during hippocampal development in nonanemic genetic mouse models, J Nutr, 143 (2013) 260-266.
[47] M.U. Muckenthaler, S. Rivella, M.W. Hentze, B. Galy, A Red Carpet for Iron Metabolism, Cell, 168 (2017) 344-361.
[48] W. Liu, J. Zhao, X. Li, Y. Li, L. Jiang, The protein kinase CaSch9p is required for the cell growth, filamentation and virulence in the human fungal pathogen Candida albicans, FEMS Yeast Res, 10 (2010) 462-470.

SUPPLEMENTAL TABLES

Table S1. List of *Saccharomyces cerevisiae* strains used in this work.

Strain	Description	Source
W303a	HTLU-2832-1B: *HIS3, TRP1, LEU2, URA3, ADE2, can1*	Fred Cross
pub1Δ	*W303a pub1::KanMX4*	This work
BY4741	*MATa, his3Δ1, leu2Δ0, met15Δ0, ura3Δ0*	Research Genetics
rpd3Δ	*BY4741 rpd3::KanMX4*	This work
dot6Δtod6Δ	*BY4741 dot6::KanMX4, tod6::HIS3MX6*	This work
stb3Δ	*BY4741 stb3::KanMX4*	Research Genetics
Sch9-HA	ACY359: *Sch9-HA (TRP1)*	Andrew Capaldi
Dot6-HA	ACY322: *Dot6-HA (KanMX)*	Andrew Capaldi
Rrp12-GFP	*BY4741 RRP12-GFP-HIS3MX6*	Joachim Griesenbeck
Rrn3-GFP	OCG0150	Olga Calvo
HA-RPC160	MW671: *MATα, ade2-101, ade2-101, lys2-801, leu2-delta1, his3delta200, ura3-52, trp1-delta63, rpc160-1::HIS3, pC160-240[TRP1 HA-RPC160]*	Francisco Navarro
rtg1Δ	*BY4741 rtg1::KanMX4*	Research Genetics
rtg2Δ	*BY4741 rtg2::KanMX4*	Research Genetics
rtg3Δ	*BY4741 rtg3::KanMX4*	Research Genetics

msn2Δmsn4Δ	*MATa*, *ade2-101, trp1Δ, msn4-Δ2::URA3, msn2-Δ3::HIS3*	Francisco Estruch

Table S2. List of oligonucleotides used for RT-qPCR in this work.

Name	***Sequence (from 5' to 3')***
ACO1-613-BglII-F	GGAAGATCTTATACTTCGCACTTTACATAT
ACO1:6-BamHI-R	CGCGGATCCCAGCATTGTATATCTATAGTA
ACT1-qPCR-F	TCGTTCCAATTTACGCTGGTT
ACT1-qPCR-R	CGGCCAAATCGATTCTCAA
SCR1-qPCR-F	TATCCAGCGTCAGCAAAGGT
SCR1-qPCR-R	CCAAATTAAACCGCCGAAG
RPB1-qPCR-F	CCAGAAGTGGTCACACCATATAA
RPB1-qPCR-R	GGTCTCCGCTATCACGAATG
RPL17A-qPCR-F	TCTTCTCCATCCCACATTGA
RPL17A-qPCR-R	GCGGCGATTCTACCTCTTT
RPL8B-qPCR-F	GGGTGTTCCATACGCCATT
RPL8B-qPCR-R	TTCGTCTTCGGCTCTGACTT
RPS16B-qPCR-F	GACGAACAATCCAAGAACGA
RPS16B-qPCR-R	AGAACGAGCACCCTTACCAC
RPL27A-qPCR-F	AGTTGCTGTCGTTGTCCGTG
RPL27A-qPCR-R	ATGGGTGAGACTTGGAACCT
18S-qPCR-F	CATGGCCGTTCTTAGTTGGT
18S-qPCR-R	ATTGCCTCAAACTTCCATCG

25S-qPCR-F	ATTGTCAGGTGGGGAGTTTG
25S-qPCR-R	GGGGCTTTTACCCTTTTGTT
tL(UAA)-qPCR-F	CTGTGGGAATACTCAGGTATCGT
tL(UAA)-qPCR-R	TTTCTCGTCTTTAGTCGGCTTC
tV(UAC)-qPCR-F	TCCTAAGCTGTCATCCGTAA
tV(UAC)-qPCR-R	ATCGAACTCGGGACCTTTG
tS(AGA)J-qPCR-F	CGAGTGGTTAAGGCGAAAGA
tS(AGA)J-qPCR-R	GGCAAAGCCCAAAAGATTTC
tK(CUU)C-qPCR-F	AATCGGTAGCGCGTATGACT
tK(CUU)C-qPCR-R	GCTCGAACCCCTAACCTTAT
LTV1-qPCR-F	CGTTTTGGTTCCTGTCTCCA
LTV1-qPCR-R	CCCTCCTACCCTTTGGTTTT
SRO9-qPCR-F	GAATCGGCAGTAGGTGAGGA
SRO9-qPCR-R	AGGTGGTTGTTGCTGTTGTG
GUA1-qPCR-F	ACTTCGCCGTTGATTTGTGT
GUA1-qPCR-R	GGACCGACCAGTTTTCTGATT
NOP14-qPCR-F	GAAGAAGGCGAAGAAAGAGGA
NOP14-qPCR-R	CAGAATCAGCAATACCGTCA
BRX1-qPCR-F	TGAAGATGGCGAAGAAGACA
BRX1-qPCR-R	GGACCACCAAATGAACC
CIT1-qPCR-F	GGTCGTGCCAATCAAGAAGT
CIT1-qPCR-R	TGCGTTCAAAGTATCCCACA
CIT2-qPCR-F	GATTTCGTGGACTTGATGAGAC
CIT2-qPCR-R	GGGACAGATAAGGTGATGATAGTG

IDH1-qPCR-F	GAGAAAACACGGAGGGTGAG
IDH1-qPCR-R	GGCGAAGTCAAAGGCAAATC
IDH2-qPCR-F	CGAGGAGGTTTTTGGCTACT
IDH2-qPCR-R	TCAGGTCCGATACCATCACC
DLD3-qPCR-F	AGGACTTGCCTTTCCCTCTG
DLD3-qPCR-R	GCTTCTCATCGTCGTGTCTCT
ACO1-qPCR-F	GCCATCAAGAGACCCATTGT
ACO1-qPCR-R	ATCCAGCGTTTCCACATTCT
DLD3-ChIP-prom-183F	GGATGACACCACTTGCCACA
DLD3-ChIP-prom-57R	GCATTTTGGCACCCTGTTCT
IDH1-ChIP-prom-150F	CCGCTTCATTGGCTTATTCTTG
IDH1-ChIP-prom-25R	AGGGAGAAGAATGAGGATAGGG
CIT2-ChIP-prom-159F	GGCCCATTATTCTCGACGTT
CIT2-ChIP-prom-85R	TGAGGAACGAACACCATATC
ACO1-ChIP-prom-186F	GAAAGGCAAGCACAAAAAGG
ACO1-ChIP-prom-64R	GAGTGAACAGAACAAGGGACAA
FUS1-ChIP-prom-F	CATGTGGACCCTTTCAAAAC
FUS1-ChIP-prom-R	AGACAGCGCGAAAAGTGACA

SUPPLEMENTAL FIGURE

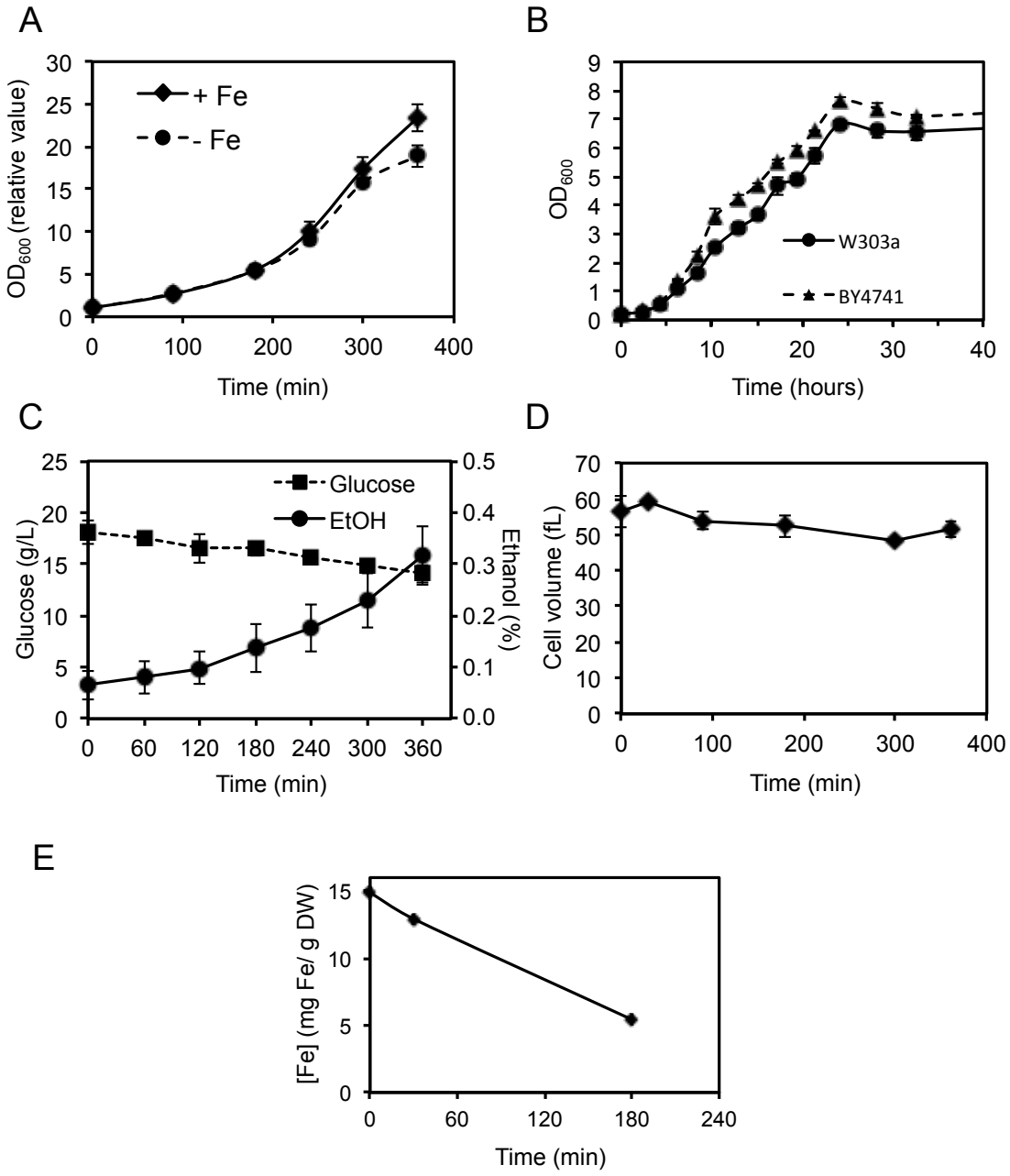

Figure S1. Determination of specific parameters during the iron deficiency experiment. (A) W303 cells were grown in SC (+Fe) and SC with 100 µM BPS (-Fe). The OD_{600nm} was measured to compare growth in both conditions. The values were referred to their respective values at time zero. **(B)** Yeast W303 and BY4741 cells were grown in SC with 100 µM BPS (-Fe). The OD_{600nm} was measured to

compare growth in both strains during the advance of iron deficiency. **(C)** Changes in glucose and ethanol levels were obtained by HPLC analysis during the progress of iron starvation. **(D)** Cell volume was determined during the growth in iron-deficient conditions as described in Materials and Methods. (E) Intracellular iron levels of W303 cells at time zero, and after 30 and 180 minutes of iron depletion. The standard deviation of at least three biologically independent replicates is represented.

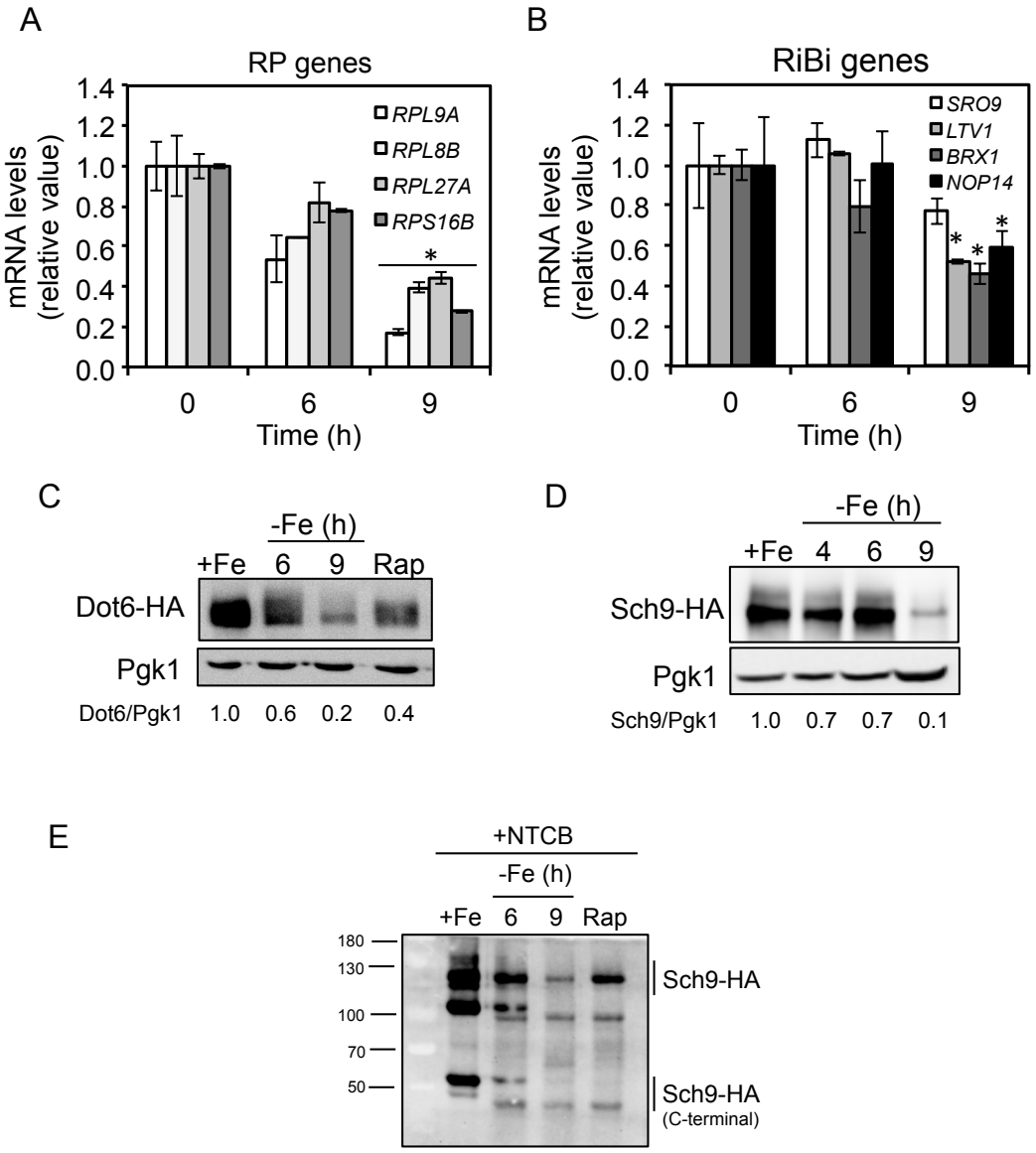

Figure S2. RP and RiBi mRNA levels, and Dot6 and Sch9 protein levels decrease in response to severe iron deficiency. (A, B) Wild type BY4741 strain was grown at 30°C in SC with 100 µM BPS (-Fe) for 9 hours. The levels of specific RP and RiBi genes were determined by RT-qPCR using specific primers. *ACT1* was used to normalize. Mean values and standard deviations from at least two independent experiments are shown and referred to time zero. **(C)** Dot6 protein

levels. Yeast cells expressing DOT6-HA were grown as in Figure 5G, and in the presence of rapamycin (200 ng/mL) for 30 minutes. Dot6-HA and Pgk1 protein levels were quantified and the Dot6-HA/Pgk1 ratio indicated. (D) Sch9 protein levels. Yeast cells expressing *SCH9-HA* were cultivated as described in Figure 5H. Total proteins were extracted and Sch9-HA and Pgk1 protein levels were determined by Western blot. The Sch9/Pgk1 ratio is shown. **(E)** Sch9 phosphorylation state. The whole Western blot corresponding to Figure 5H is shown.

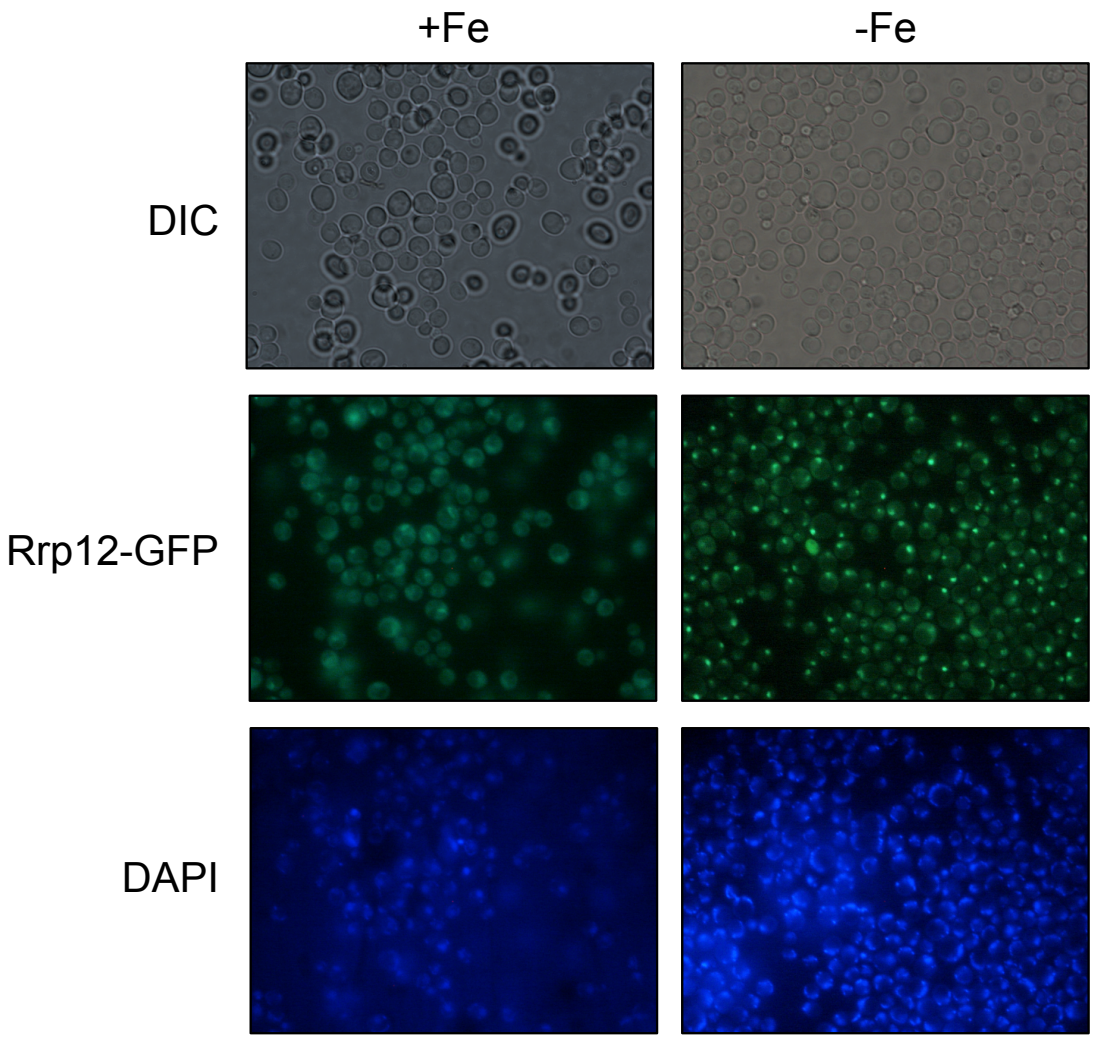

Figure S3. Rrp12 localizes to the nucleus in iron-deficient conditions. Yeast cells expressing *RRP12-GFP* were grown in SC (+Fe) and SC with 100 μM de BPS (-Fe) and were visualized after 9 hours of growth. DIC, differential interference microscopy. DAPI, 4',6-diamidino-2-phenylindole.

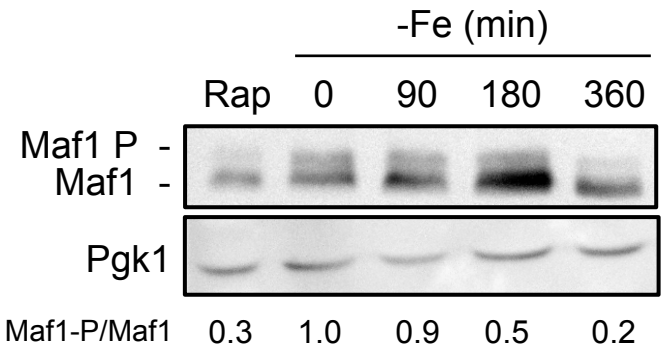

Figure S4. Maf1 is dephosphorylated during the iron deficiency progress. W303 cells were grown as described in Figure 1A. The phosphorylation state of Maf1 protein was analyzed by immunoblotting using an anti-Maf1 antibody. Pgk1 protein levels were used as a loading control.

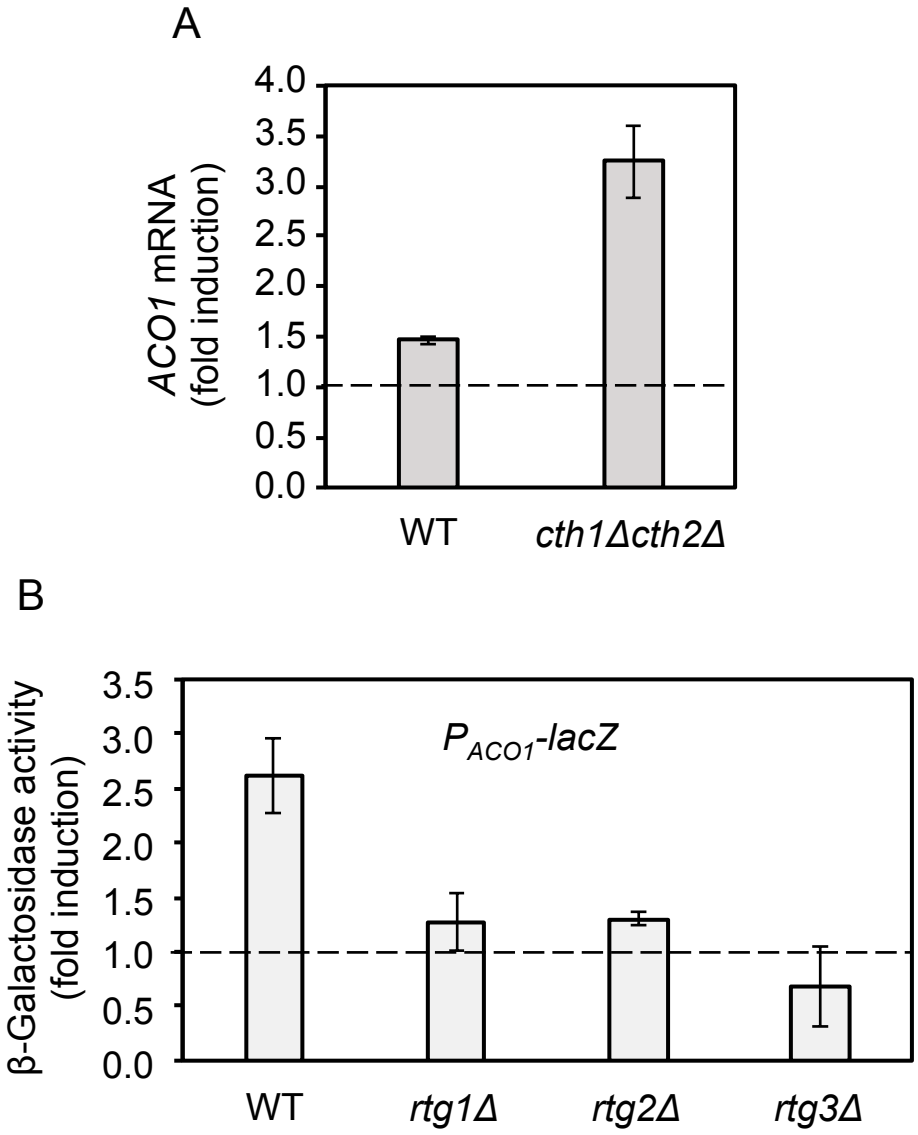

Figure S5. *ACO1* is transcriptionally and post-transcriptionally regulated in response to iron deficiency. (A) Wild type BY4741 and *cth1Δcth2Δ* strains were grown in SC (+Fe) and SC with 100 μM BPS (-Fe) for 9 hours. *ACO1* mRNA levels were determined by RT-qPCR. Mean values of fold induction in iron deficiency and standard deviations from at least two independent experiments are shown. **(B)** Wild type BY4741, *rtg1Δ, rtg2Δ and rtg3Δ* strains transformed with the plasmid P_{ACO1}-lacZ were grown at 30 °C in SC-ura (+Fe) and SC-ura with 100 μM BPS (-Fe) for 9 hours. β-Galactosidase assays were carried out as described in Materials and Methods. Mean values of fold induction in iron scarcity and standard deviations from at least two independent experiments are shown